coatings

MDPI

Review

Polymer Waveguide-Based Optical Sensors—Interest in Bio, Gas, Temperature, and Mechanical Sensing Applications

Svetlana N. Khonina [1,2], Grigory S. Voronkov [3], Elizaveta P. Grakhova [3], Nikolay L. Kazanskiy [1,2], Ruslan V. Kutluyarov [3] and Muhammad A. Butt [1,*]

[1] Samara National Research University, 443086 Samara, Russia
[2] IPSI RAS-Branch of the FSRC "Crystallography and Photonics" RAS, 443001 Samara, Russia
[3] Ufa University of Science and Technology, 32, Z. Validi Street, 450076 Ufa, Russia
* Correspondence: butt.m@ssau.ru

Abstract: In the realization of photonic integrated devices, materials such as polymers are crucial. Polymers have shown compatibility with several patterning techniques, are generally affordable, and may be functionalized to obtain desired optical, electrical, or mechanical characteristics. Polymer waveguides are a viable platform for optical connectivity since they are easily adaptable to on-chip and on-board integration and promise low propagation losses <1 dB/cm. Furthermore, polymer waveguides can be made to be extremely flexible, able to withstand bending, twisting, and even stretching. Optical sensing is an interesting field of research that is gaining popularity in polymer photonics. Due to its huge potential for use in several industries, polymer waveguide-based sensors have attracted a lot of attention. Due to their resilience to electromagnetic fields, optical sensors operate better in difficult situations, such as those found in electrical power generating and conversion facilities. In this review, the most widely used polymer materials are discussed for integrated photonics. Moreover, four significant sensing applications of polymer-waveguide based sensors which include biosensing, gas sensing, temperature sensing and mechanical sensing have been debated.

Keywords: polymer; waveguide; optical sensor; temperature sensor; biosensor; gas sensor

check for updates

Citation: Khonina, S.N.; Voronkov, G.S.; Grakhova, E.P.; Kazanskiy, N.L.; Kutluyarov, R.V.; Butt, M.A. Polymer Waveguide-Based Optical Sensors—Interest in Bio, Gas, Temperature, and Mechanical Sensing Applications. *Coatings* **2023**, *13*, 549. https://doi.org/10.3390/coatings13030549

Academic Editor: Mohor Mihelčič

Received: 2 February 2023
Revised: 22 February 2023
Accepted: 1 March 2023
Published: 3 March 2023

Copyright: © 2023 by the authors. Licensee MDPI, Basel, Switzerland. This article is an open access article distributed under the terms and conditions of the Creative Commons Attribution (CC BY) license (https://creativecommons.org/licenses/by/4.0/).

1. Introduction

Polymers have the potential to be useful for many passive and active sub-components. One benefit of polymers over other types of materials is that their physical and optical characteristics may be greatly customized by adjusting the composition and level of polymerization. By including the proper molecular moieties in the polymer chain or as side pendants, functionality may be introduced [1]. Different techniques may be used to process polymers, such as solution and gas-phase deposition, and they can be made compatible with substrate chemistry by appropriate surface functionalization (including inorganic building blocks). Large-scale, inexpensive production of polymers is also a possibility [2]. The optical waveguide (WG) is one of the fundamental components of integrated photonics [3–6]. Polymer WGs can operate in either single-mode (with core diameters between 2 µm and 5 µm) or multimode (with core dimensions generally between 30 µm and 500 µm) regimes. They are both entirely consistent with the matching optical fiber type due to the similar mode field diameter. Numerous methods, including photolithography [7], flexographic and inkjet printing [8], nanoimprint lithography [9,10], femtosecond laser processing [11], and hot embossing [12], can be used to create these WGs. A stamp structure is transferred from a stamp onto a substrate through the hot embossing process, which is a replication process. The method is appropriate for replicating structures with a millimeter to nanoscale size. Due to its potential for mass production at low cost and integration with roll-to-roll processes, hot embossing is a desirable manufacturing method for optical applications [13]. By using sustainable and efficient hybrid lithography, a three-dimensional polymer WG

with a taper structure was exhibited and created [14]. A polymer WG and a polymer taper structure were created using grayscale lithography and hybrid lithography, respectively. Gray-scale lithography was intended for laser ablation and shadow aluminum evaporation. The laser strength, the rate of ablation, and the thickness of the aluminum may all be adjusted to alter the length of the grayscale zone, which ranges from 20 to 400 µm [14].

Due to their flexible processibility and integration over inorganic counterparts, polymer optical WG devices are crucial in several rapidly evolving broadband communications domains, including optical networking, metropolitan/access communications, and computer systems [15]. Owing to their many benefits, they are also a perfect integration platform for the insertion of foreign material systems like YIG (yttrium iron garnet) and lithium niobate in addition to semiconductor devices like lasers, detectors, amplifiers, and logic circuits into etched grooves in planar lightwave circuits to enable full amplifier modules or optical add/drop multiplexers on a single substrate. Additionally, optical polymers may be vertically combined to produce 3D and even all-polymer integrated optics because of their flexibility and durability combination [14].

Polymer WG-based optical sensors can be competitors to devices based on photonic integrated circuits (PICs). Such devices are mainly manufactured based on MPW (multi-project wafer) on SOI, SiN platforms, or based on Group III–V semiconductors, primarily InP or GaAs. Type III–V platforms can provide a wide range of active devices, but they are poorly applicable to passive elements due to high attenuation and low contrast [16–18]. Figure 1 shows the emission wavelength coverage of semiconductor lasers based on III–V platforms [19]. One can see that their emission region is lower than the Si transparency window. The transparency range of a polymer WGs depends on the specific polymer material being used. In general, the transparency range is in the near-infrared (NIR) region of the electromagnetic spectrum, usually from 700 nm to 1700 nm. Therefore, one can easily combine them with III–V group light sources in the sensing system's design. However, some polymers have higher transparency windows extending into the visible region or even beyond the short-wave infrared (SWIR) region [20,21]. It is also worth noting that the transparency range of polymer WGs can be affected by various factors such as processing conditions, doping, and absorption or scattering losses. SOI platforms, which are well-compatible with traditional CMOS electronics, have high contrast and small allowable bend radii [22], making it possible to design small-sized passive sensor devices but not active components. For example, a sensor based on a Mach–Zehnder interferometer (MZI) with a double-slot hybrid plasmonic WG [23] provides a high sensitivity of up to 1061 nm/RIU in liquid refractometry. The micro-ring resonator-based sensors' sensitivity on the SOI platform is less than 100 nm/RIU. However, the application of a subwavelength grating micro-ring makes it possible to achieve a sensitivity of 672.8 nm/RIU [24,25]. Hybrid integration significantly expands the capabilities of the SOI and III–V platforms, allowing the design of complex sensing systems, including active devices [26,27]. It is also possible to expand the capabilities of the SOI platform using IMOS (indium phosphide membrane on silicon) technology [28].

The paper is organized in the following manner. Section 2 provides a piece of information on the characteristics of polymer WGs. There are several polymer materials commercially available and being used in research for the development of photonic devices as discussed in Section 3. The extraordinary optical properties of these polymer materials include low optical losses at operating wavelengths, well-controlled and tunable refractive indices, resistance to temperature and chemicals, mechanical stability in a variety of environments, and environmentally friendly fabrication techniques. Afterward in Section 4, polymer WG-based sensors are discussed. We have dedicated our research to polymer WG-based biosensors (Section 4.1), gas sensors (Section 4.2), temperature sensors (Section 4.3), and mechanical sensors (Section 4.4), which are at present the main focal point of investigation. The paper finishes with a brief conclusion and outlook as presented in Section 5. The applications presented in this paper are shown in Figure 2.

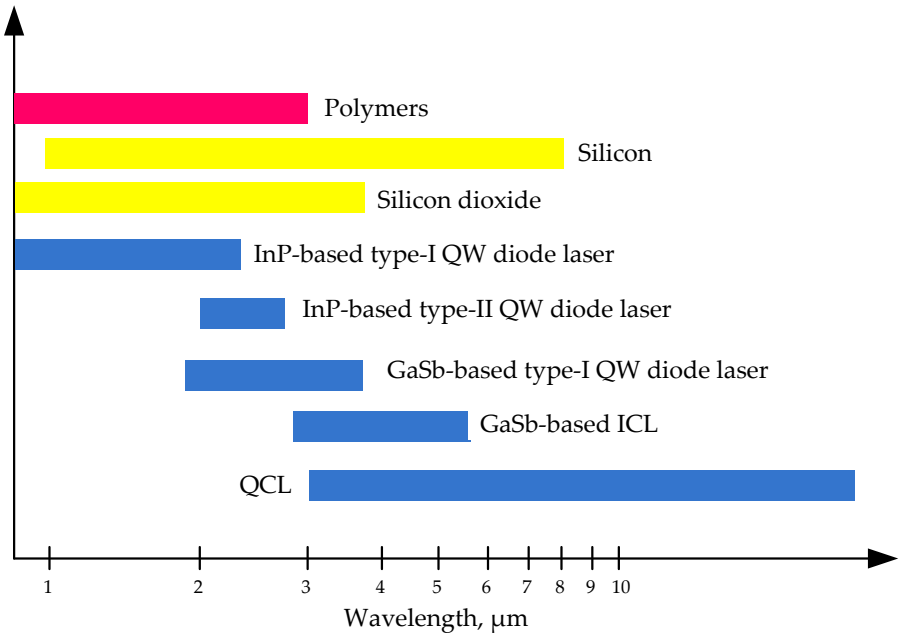


Figure 1. Transparent window of polymers, silicon, and silicon dioxide, and emission wavelength coverage of semiconductor lasers based on different III–V active regions. InP-based type-I, type-II, and GaSb-based type-I quantum well (QW) diode lasers, GaSb-based interband cascade lasers (ICLs), and quantum cascade lasers (QCLs) are included [19].

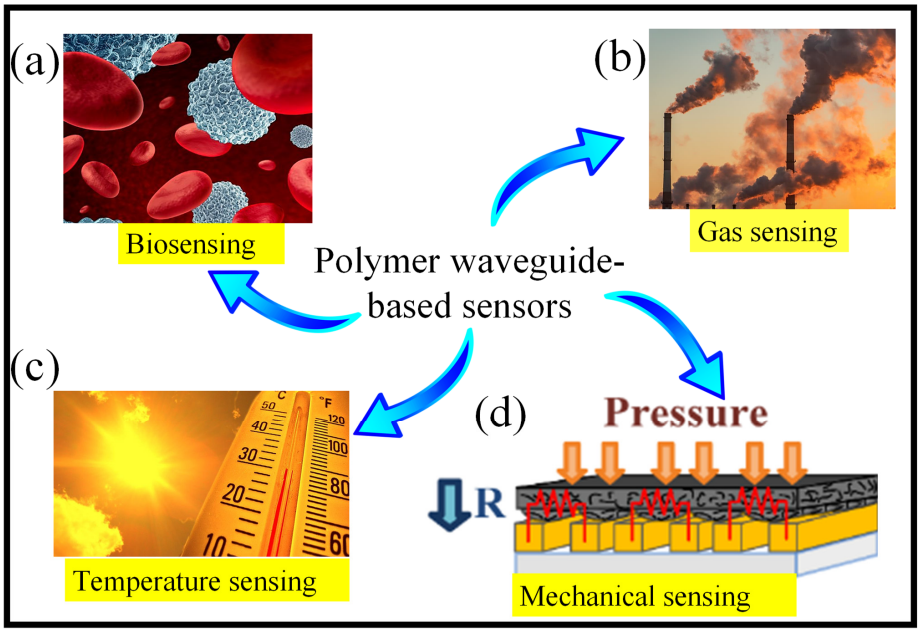


Figure 2. Polymer WG-based sensors employed in (**a**) biosensing [29], (**b**) gas sensing [30], (**c**) temperature sensing [31], and (**d**) mechanical sensing applications [32], are discussed in this review.

2. Characteristics of Polymer Waveguides

Using straightforward spin-coating processes, low-temperature processing, and compatibility with semiconductor electronics, optical polymers enable the flexible, large-area, and inexpensive production of WG devices [13]. These WGs are relatively cheap to produce compared to other materials such as glass or silicon. This makes them a popular choice for cost-sensitive applications. Glass, quartz, oxidized silicon, glass-filled epoxy printed circuit board substrate, and flexible polyimide film are just a few examples of the numerous rigid

and flexible substrates that can be employed. Film thicknesses between 0.1 and 100 microns can be achieved by adjusting the polymer/solvent ratio and spin speed in the film coating process. Contrary to other optical material systems, polymers are created and designed by chemically altering their component molecules to have the desired properties, such as melt or solution processibility in the form of monomers or prepolymers, enhanced mechanical properties from photo- or thermo-crosslinking, and matched refractive indices between the core and cladding layers. Polymer materials have high flexibility, making them ideal for applications where flexible WGs are required, such as flexible displays or wearable devices [33]. These WGs are much lighter than traditional glass or silicon WGs, making them easier to integrate into portable or mobile devices.

Additionally, these characteristics are modifiable by formulation changes. In addition to the traditional photoresist patterning, there are other methods for forming polymer WGs, such as direct lithography, soft lithography, embossing, molding, and casting. This enables the quick and inexpensive structuring of components like active films, Faraday rotators, or half-wave plates for the creation of WGs as well as material removal for grating. This adaptability also makes polymers an excellent hybrid integration platform, allowing for the insertion of semiconductor devices like lasers, detectors, and logic circuits into an etched groove in a planar lightwave circuit to facilitate full amplifier modules or optical add/drop multiplexers on a single substrate. These foreign material systems include Yttrium iron garnet (YIG), lithium niobate, and foreign material systems [34].

The fact that polymeric materials' refractive indices change more quickly with temperature than more traditional optical materials like the glass is a key distinction between the two. When ambient temperature increases, the refractive index of the polymer material drops at a rate of $10^{-4}/^{\circ}C$, which is significantly—faster than inorganic glasses. As opposed to the interferometric devices that are required in silica-on-silicon, for example, this large thermo-optic coefficient and poor thermal conductivity allow for the realization of thermo-optic switches with low power consumption, digital thermo-optic switches, and thermo-optic switches based on adiabatic WG transitions.

Polymers are more sensitive to humidity compared to inorganic materials. The impact of humidity on the refractive index may also be examined using the return-loss method [35]. If the core and cladding modifications were different, the refractive index change caused by humidity would have an impact on single-mode WG performance. It would also have an impact on the device's return loss if index matching were utilized as a return loss reduction technique. Devices like Bragg gratings and AWGs may function differently even though the core and cladding change is the same because the humidity may alter the WG's effective index.

Many optical systems rely on the exclusion of any wavelength-dependent optical effects outside those that were physically intended. Material dispersion should thus typically be avoided. The values for the polymers on the order of 10^{-6} nm^{-1} are substantially lower than those for semiconductors or doped glasses, although being equivalent to those for SiO_2 [7]. Because polymeric materials are susceptible to yellowing with thermal aging, the thermal stability of optical qualities is a crucial property for practical applications. Such aging is often caused by the production of partly conjugated chemical groups, which exhibit wide UV absorption bands and weaken over the visible spectrum. The chemical composition of the original polymer has a significant impact on this yellowing.

Polymer materials have a limited operating temperature range, which can make them unsuitable for high-temperature environments. These materials are more prone to mechanical degradation, such as cracking or breaking, compared to other materials such as glass or silicon. They are also sensitive to environmental factors such as moisture, heat, and UV light, which can affect the performance and longevity of the WG. Overall, polymer WGs have some advantages such as low cost and flexibility, but also have some limitations in terms of optical quality and mechanical stability. Whether or not to use polymer WGs will depend on the specific requirements and constraints of the application.

3. Polymer Materials for Integrated Optics and Fabrication Methods

In the past, optical crystals like lithium niobate [36], lithium tantalate [37], and rubidium titanyl phosphate [38,39] as well as semiconductors like silicon [4,5,40], silicon nitride [41,42], indium phosphide [43,44], III–V compound, and silica have been utilized to create optical WGs. In recent years, there has been much study on highly integrated optics and photonic devices made of polymers. Polymer materials, as compared to the materials mentioned above, have easier manufacturing procedures, which result in produced optical devices with much-reduced material and production costs [45]. As a result, new types of polymers for optical and photonics uses have been produced in several laboratories throughout the world in recent decades, and some of them are now accessible on the market. These materials include UV-curable epoxy polymers Su-8, EpoCore/EpoClad [46,47], siloxane LIGHTLINKTM XP-6701A core, LIGHTLINKTM XH-100145 clad, and benzocyclobutene (Dow Chemical, Midland, MI, USA) Polymers [48], ZPU resin, and polymers (ChemOptics Inc., Daejeon, Republic of Korea) [49], OrmoClear®FX (micro resist technology GmbH), and SUNCONNECT are examples of inorganic–organic hybrid polymers (Nissan Chemical Ltd., Tokyo, Japan) [20,50], Truemode Backplane Polymer (Dow Corning, Midland, MI, USA) [51], UV exposure optical elastomer OE-4140 core, and OE-4141 cladding (Exxelis, Ltd., Washington, DC, USA) [52], Sylgard 184, LS-6943, polydimethylsiloxane (PDMS) [53], etc.

Polymethyl Methacrylate (PMMA) is a widely used polymer material for optical WGs due to its transparency, high refractive index, and low cost. Polycarbonate (PC) is a thermoplastic polymer that is commonly used for optical WGs due to its high transparency, high mechanical strength, and good thermal stability. Polystyrene (PS) is a transparent polymer that is widely used for WGs due to its low cost, easy processability, and good transparency in the visible and near-infrared regions of the spectrum. Polyimide (PI) is a heat-resistant polymer that is widely used for high-temperature applications due to its excellent mechanical stability, high transparency, and high refractive index. Polyethylene (PE) is a flexible and lightweight polymer that is widely used for applications such as fiber-optic sensing and flexible displays due to its low cost and high transparency. Polyvinyl chloride (PVC) is a low-cost polymer that is widely used for optical WGs due to its good processability and high transparency in the visible and near-infrared regions of the spectrum. Cytop and cyclic olefin copolymer (COC) polymer materials are widely used for WGs in optical communication systems and other optical applications. These materials have a low-loss, high-refractive-index polymer material that offers a combination of transparency, high mechanical strength, and good thermal stability. They are some of the most used polymer materials for optical WGs, but many other polymers can also be used, depending on the specific requirements of the application.

These polymer materials have exceptional optical qualities, for instance, low optical losses at working wavelengths (including in the infrared spectrum), well-controlled and tunable refractive indices, resistance to temperature and chemicals, mechanical stability in a variety of environments, and environmentally friendly fabrication methods [54,55]. Polymers are used to create common types of fiber sensors: fiber Bragg gratings (FBG) [56,57], surface plasmon resonance (SPR) sensors [58,59], and intensity variation-based sensors [60,61]. To realize optical and photonic devices, optical planar WGs are essential building blocks. Several distinct manufacturing methods for polymer optics WG devices have been documented. These fabrication techniques include the use of mask photolithography in conjunction with wet etching [62], photo-resist patterning and reactive ion etching [63], two-photon polymerization [64], laser direct writing [47], electron beam writing [65], flexographic and inkjet printing [8], the hot embossing process [66–68], photo-bleaching [69], and others. These processes need numerous processing steps, which can result in lengthy fabrication periods and poor yield. For mass production, technologies like stamping processes [70] are being researched. The roll-to-roll (R2R) nanoimprint lithography technologies [71,72] and roll-to-plate nanoimprinting are two examples of these techniques. Polymers, which are excellent material candidates for applications needing low-cost mass manufacturing,

can be used with these roller-based methods [72]. Flexible electronics are created using these methods [73]. Additionally, current research is looking into potential uses in optics and photonics. Additional information on thin-film coating processes can be found in [13]. We should notice that the soft-lithography fabrication process provides high geometrical accuracy [74], which guarantees sensors' fabrication reproducibility.

Several researchers have looked at the development of optical WGs using hot embossing in recent years [12,66,68,75]. Numerous stamp production methods, including LIGA technology, photolithography, micro-machining, and etching, were investigated. The investigation of several polymer materials also included thermoplastics and photoresists [76]. The manufactured WGs were utilized for optical communication and sensing applications and worked in the single-mode and multi-mode regimes. The WG transmission loss varies from several dB/cm to values under 1 dB/cm depending on the embossing stamp and the polymer materials. Despite its advantages, the hot embossing process also has some disadvantages such as requiring specialized equipment, which can be expensive and may not be readily available for all users. The hot embossing process requires high temperatures, which can cause thermal stress and degradation of the polymer material. It requires complex tooling, such as molds and stamps, which can be difficult to design and fabricate. Moreover, it is limited to certain types of polymer materials such as thermoplastics, which may not be suitable for all applications. The surface finish of the embossed component may not be as high as other fabrication methods, which can affect the optical properties of the component and can result in non-uniform embossing, which can then affect the performance of the component. Furthermore, it may not be suitable for high-volume production, as it is a relatively slow and labor-intensive process. Table 1 shows the most frequently used polymer materials and their physical characteristics.

Table 1. Most commonly used polymer materials and their characteristics.

Polymer	Chemical Formula	Young Modulus	Optical Loss	Transparency Region, nm	Refractive Index
NOA 73	N/A	11 MPa [77]	N/A	370–1250 [78]	1.559 [78]
PDMS	$(CH_3)_3SiO[Si(CH_3)_2O]nSi(CH_3)_3$ [79]	1.32–2.97 MPa [80]	0.027 dB/cm [81]	400–1600 [81]	$n(T) = 1.4176 - 4.5 \times 10^{-4}T$ [82]
PMMA [9,83]	$(C_5H_8O_2)n$ [84]	3–3.7 GPa [85]	2.5 dB/cm [83]	400–700 with C-H absorption peak at 630 nm [86]	1.48–1.505 [87]
NOA 68	N/A	N/A	N/A	450–1250 [88]	1.54 [88]
COC	cyclic olefin copolymer	29–237 MPa [89]	0.5 dB/cm (830 nm); 0.7 dB/cm (1550 nm) [90]	N/A	1.5–1.54 [90]
SU-8	epoxy polymer	4.54 GPa at 19 kHz to 5.24 GPa at 318 kHz [91]	1.36 and 2.01 dB/cm (TE_{00} and TM_{00}) [46]	N/A	1.67 at UV [92]
Ormocer	inorganic-organic hybrid polymers	1–17,000 MP [93]	0.64 dB/cm [94]	N/A	From 1.5382 to 1.59 at 633 nm [95]
ZIF-8	2-Methylimidazole zinc salt	3 GPa [96]	N/A	N/A	1.355 ± 0.004 at 589 nm [97]
PHMB	polihexanide	N/A	N/A	N/A	1.48–1.5 [98]
BCB	benzocyclobutene	9.58 GPa [99]	0.81 dB/cm at 1300 nm [100]		1.5589 at λ = 632 nm; 1.5489 at λ = 838 nm [101]
FSU-8	fluorinated epoxy resin	N/A	N/A	N/A	1.495 to 1.565 at 1550 nm [102]
NOA 63	N/A	N/A	N/A	350–1250	1.56 [103]
PEI	polyethylenimine	3.5–3.6 GPa [104]	N/A	400–800 [27,105]	1.66 at 546 nm [106]
PSS	polystyrene sulfonate		N/A	N/A	
PAH	polyallylamine hydrochloride	100 MPa [107]	N/A	N/A	1.51 at 550 nm [108]
Ma-P 1205	n/a	N/A	N/A	N/A	1.644 at 633 nm [109]
PMATRIFE	poly(2,2,2) MethAcrylate of TRIFluoro-Ethyle	N/A	N/A	N/A	1.409 [110]
PC [33]	plastic polycarbonate	N/A	10 dB/m	750–850	1.586 [111]
CYTOP [33]	amorphous perfluorinated polymer		10 db/km	950–1100	1.34 at 587.6 nm
PDLLA	poly(D,L-lactide)	N/A	From 0.4 dB/cm on 500 nm to 0.12 dB/cm on 800 nm with C-H adsorbtion peak at 720–740 nm [45]	500–850 [86]	N/A

Rapid and extensive duplication of structures with dimensions ranging from the microscale to centimeter scale is possible using hot embossing [68]. Figure 3 provides a detailed illustration of the fabrication processes. The top and lower phases, respectively, were initially covered with a structured stamp and a PMMA sheet. Then, they were heated to 140 °C, which is both lower than the PMMA melting point and higher than the glass

transition temperature. The PMMA sheet was in a rubber condition at this temperature, making it appropriate for the ensuing embossing of structural patterns. The structural stamp was applied with an embossing force to the PMMA sheet during the embossing process. A further cooling procedure was used to maintain the embossing force while chilling the stamp and PMMA sheet. A further cooling procedure was used to maintain the embossing force while chilling the stamp and PMMA sheet. The embossing force was withdrawn once the temperature reached the demolding temperature (50 °C). Manual separation of the PMMA sheet and stamp is possible [68].

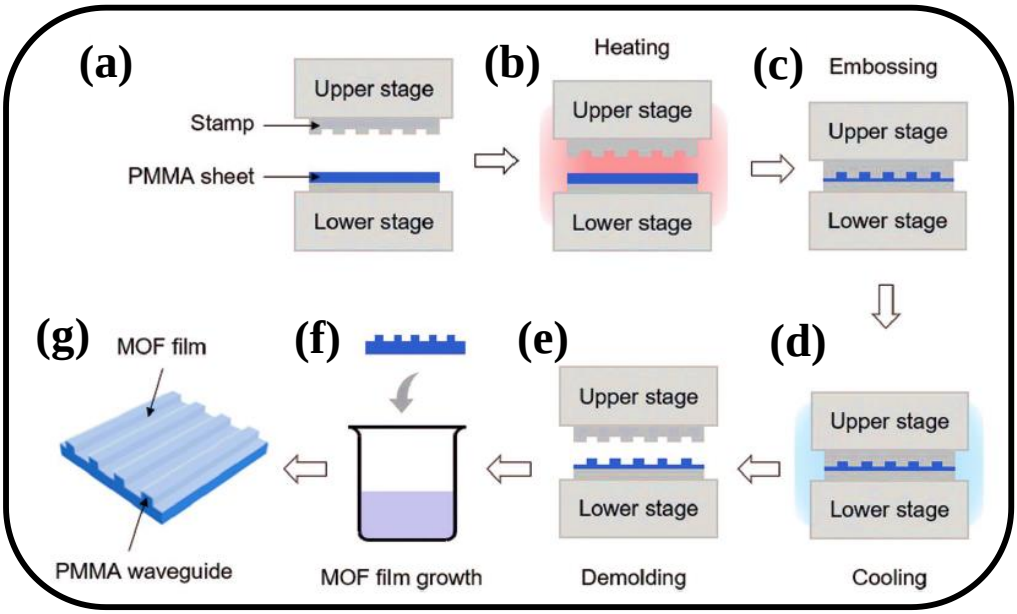


Figure 3. Manufacturing process of MOF-coated WGs by employing hot embossing, (**a**–**g**) Step by step fabrication process of PMMA based WG [68].

4. Polymer WG-Based Sensors

The characteristics and needs of a certain application will determine how a sensor is designed for that purpose. It is helpful to list the qualities that one would need in a perfect sensor for chemical and biological species. In a perfect world, the sensor would have sufficient sensitivity (in certain situations down to the level of a single molecule) and a wide dynamic range. High selectivity for the target species and resistance to sample-matrix interferences should also be present. A perfect sensor would also be suited for multicomponent measurements, have a quick reaction time, be reversible, and have high long-term stability. The ideal sensor should also be capable of self-calibration and be strong, dependable, easy to make, affordable, and have a compact size.

The most significant benefit of optical sensors over other types is their broad range of applications: optical sensors may detect analytes for which other (bio)chemical sensors are ineffective [112]. Additionally, optical sensors can be used for "indirect" analyte identification, which makes use of an auxiliary reagent, as well as "direct" analyte detection, in which the spectroscopic characteristics of the analyte are detected. Such a reagent experiences a modification in an optical property, such as elastic or inelastic scattering, optical path length, absorption, luminescence intensity, luminescence lifespan, or polarization state, when it interacts with the analyte species. This type of indirect detection is essential because it merges chemical selectivity with the spectroscopic measurement's capabilities and frequently overcomes interference issues that would otherwise be problematic.

There are several subcategories of optical sensors. There are "intrinsic" and "extrinsic" sensors, for example. A WG is simply utilized as a light link to connect external instruments to a sampling point or an optical sensing element in an extrinsic sensor. In biomedicine, environmental monitoring, process control, and safety, extrinsic sensors are already widely

employed [113]. Due to several appealing qualities they possess, including simplicity, electrical passivity, inherent safety, chemical robustness, thermal tolerance, compatibility with telemetry, and use of a common technology to produce sensors intended for various (bio)chemical and physical measurements, they have found success in both commercial and practical purposes. Extrinsic sensors may also frequently be made simpler, work with in vivo applications, and be applied in situations that are contaminated by electromagnetic and microwave waves.

In an intrinsic sensor, the WG itself contributes to the conversion of (bio)chemical data into an analytical signal that is usable [114]. In addition to the common qualities of most extrinsic sensors, intrinsic sensors offer a variety of useful features [115,116]. By using evanescent-wave-based optical discrimination, intrinsic sensors may be employed to study interfacial processes and thin films. By adjusting the parameters of the waveguiding configuration and, in the case of indirect sensors, the parameters of immobilized reagents, they also provide flexibility in the selection of their sensing mode and their analytical properties. For instance, the architecture of the WG, its cladding, and any reagents nearby the WG can all affect how much an evanescent wave interacts [117,118]. The choice of the physical, chemical, or biological characteristics of the analyte species to be monitored is often the first stage in the construction of a good sensor. One could decide to analyze an analyte's absorption, fluorescence, or Raman spectra, for instance. This decision will determine the sensor's instrumental needs as well as its analytical performance. It is frequently helpful to take into consideration a combination of detection techniques since doing so may frequently result in a significant performance gain. A fluorescence-based sensor combined with time-resolved detection, for instance, can enhance a sensor's selectivity, sensitivity, and long-term stability.

Surface plasmon resonance (SPR) [119], grating, micro-ring [120–122], and MZI [123] structures are only a few of the basic structural types found in polymer optical WG sensors, as shown in Figure 4a–d [124–126]. A commercial chemical detection device based on prism-coupling technology is included in the SPR structure. Its limitations include susceptibility to temperature and test media composition, as well as optical loss due to the gold film. The grating structure has a very low grating period—only a few hundred nanometers—but it also has demanding production and spectral analysis constraints. Temperature and outside stress might affect longer grating times. The micro-ring structure's radius is many tens of micrometers, making it desirable for sensor downsizing. The equivalent contact length of the WG and test medium is greatly increased by the optical signal resonance phenomena to provide adequate sensitivity. Nevertheless, it is difficult to manage the coupling distance between the micro-ring and straight WG without using a high-precision construction procedure. The micro-ring may also result in more bending loss.

In the MZI structure, one WG branch acts as the sensing arm and the other branch as the reference arm. The evanescent field of the light wave in the core layer may be made to make contact with the test medium by detaching the upper cladding layer of the WG from the sensing arm [127]. The refractive index (RI) of the test medium varies, which affects how the optical fields between the sensing and reference arms are phased. The output optical power varies because of the phase shift. The MZI construction is affordable, simple to construct, and capable of simultaneous multi-channel identification without the need for spectral detection. An integrated MZI-based methane sensor that is covered in a styrene-acrylonitrile film that contains cryptophane-A is presented [126]. A supramolecular molecule called cryptophane-A that can selectively trap methane increases sensitivity by a factor of 17 when it is present in the cladding [126].

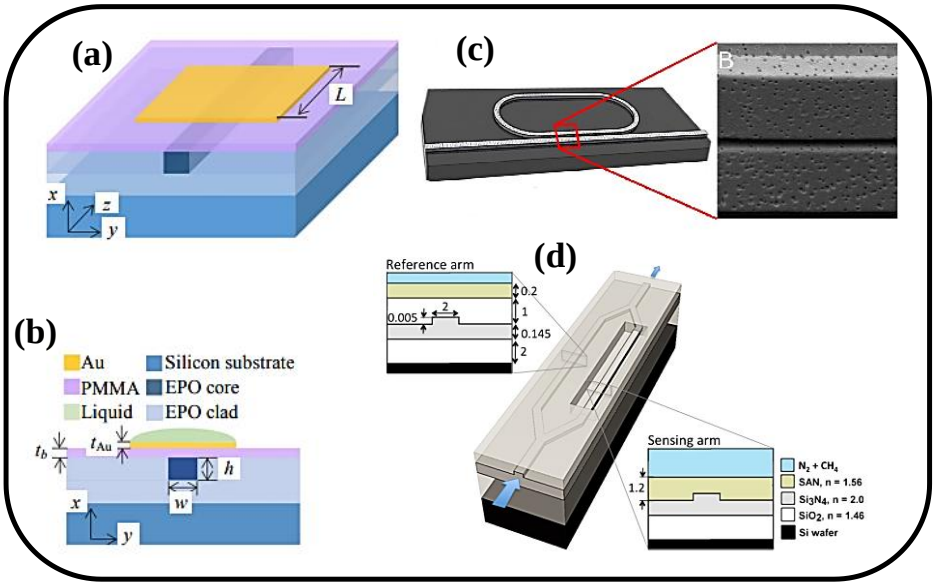


Figure 4. Different types of sensors based on polymer WGs, (**a**,**b**) SPR [124], (**c**) Micro-ring resonator [125], (**d**) MZI structure [126].

4.1. Polymer WG-Based Low-Cost Biosensors

Today, biosensors are widely used in biological diagnostics as well as a variety of other fields, including forensics, environmental monitoring, food control, drug development, and point-of-care monitoring of illness progression [128,129]. The creation of biosensors may make use of a broad variety of methodologies. As a result of their interaction with high-affinity biomolecules, a variety of analytes may be sensitively and specifically detected [130,131]. Every biosensor contains a particular set of static and dynamic properties [132,133]. The efficiency of the biosensor is enhanced by the optimization of these properties [134].

4.1.1. Selectivity

Perhaps the most crucial component of a biosensor is selectivity. A bioreceptor's selectivity refers to its capacity to identify a particular analyte in a sample that contains various admixtures and impurities. The interplay of an antigen and an antibody is the greatest illustration of selectivity. Antibodies often serve as receptors and are immobilized on the transducer's surface. The antigen is then introduced to a solution (often a buffer including salts), which is subjected to the transducer, where antibodies only bind with the antigens. Selectivity is the key factor to be taken into account while developing a biosensor [135].

4.1.2. Limit of Detection

The limit of detection (LOD) of a biosensor is the lowest conc. of analyte that it can detect [136]. A biosensor is necessary for several medical and environmental monitoring applications to confirm the existence of traces of analytes in a sample at analyte conc. as low as ng/mL or even fg/mL. For instance, prostate cancer is linked to blood levels of the prostate-specific antigen (PSA) of 4 ng/mL, for which doctors recommend biopsy procedures. As a result, LoD is thought to be a key characteristic of a biosensor.

4.1.3. Stability

The biosensing system's stability refers to how susceptible it is to environmental perturbations within and outside of it. A biosensor under study may experience a drift in its output signals because of these disruptions [137]. This may result in a conc. measurement inaccuracy and compromise the biosensor's quality and precision. In situations where a biosensor needs lengthy incubation periods or ongoing monitoring, stability is the most

important component. The reaction of electronics and transducers may be temperature-sensitive, which might affect a biosensor's stability. To achieve a steady response from the sensor, proper tuning of the electronics is necessary. The degree to which the analyte attaches to the bioreceptor—the affinity of the bioreceptor—can also have an impact on stability. High-affinity receptors promote the analyte's covalent or strong electrostatic connection, which strengthens a biosensor's stability. The deterioration of the bioreceptor over time is another element that has an impact on a measurement's stability.

4.1.4. Repeatability

The biosensor's repeatability refers to its capacity to provide the same results under identical testing conditions. The transducer and electronics in a biosensor are precise and accurate, which defines repeatability. When a sample is tested more than once, accuracy refers to the sensor's capability to offer a mean value that is near to the real value while precision refers to the sensor's ability to produce identical findings every time. The inference built on a biosensor's response is very reliable and robust when the signals are reproducible [137].

The optical sensors based on evanescent wave monitor changes in the RI. These sensors make use of the confinement of the electromagnetic waves in a dielectric and/or metal structure to generate a propagating or localized electromagnetic mode. The evanescent wave is created when a portion of the confined light disperses into the surrounding medium as shown in Figure 5. Local changes in the optical properties of the excited electromagnetic mode, most significantly a change in the effective RI, are brought on by RI shifts in the surrounding medium through this evanescent wave [116]. When a receptor layer is affixed to the guiding structure's surface, the corresponding analyte is exposed to it, and the resulting (bio)chemical interactions between them change the RI locally. The interaction's amplitude may be measured by comparing it to the analyte's conc. and the interaction's affinity constant. The evanescent wave only reaches the exterior medium up to hundreds of nanometers and perishes exponentially; consequently, the background from the external medium will be little impacted. As a result, only variations near the sensor surface will be noticed.

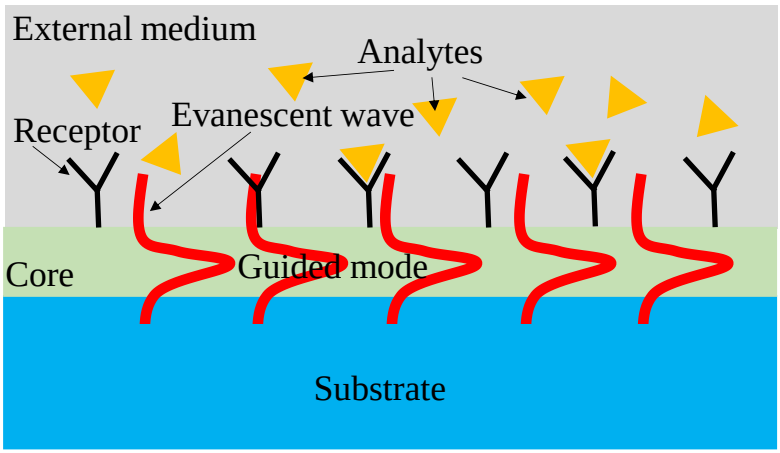


Figure 5. Evanescent field sensing mechanism.

The interferometric evanescent wave sensing technique is used by planar-integrated optical biosensors to provide highly sensitive label-free detection of biomolecules. Using injection molding and spin-coating, a novel polymer WG device design is proposed that enables the production of disposable sensor chips at a cheap cost [138]. To couple light into and out of the biosensor, surface grating couplers and lateral tapers were included. By adding a thin layer of inorganic high-index material to these polymer gratings, the coupling strength is improved, allowing for grating size reduction and effective lateral tapering into single-mode WGs [138].

For detecting effective medication doses of ginkgolide A for the suppression of pulmonary microvascular endothelial cell (PMVEC) apoptosis, a fluorinated cross-linked polymer Bragg WG grating-based optical biosensor is developed [139]. PMMA was created as the sensing window cladding and fluorinated photosensitive polymer SU-8 (FSU-8) as the sensing core layer. Pharmacological experiments were used to examine and examine the ginkgolide A medication conc. range that was most efficient for inhibiting PMVEC apoptosis (5–10 g/mL). The device's framework was built to be created and manufactured using direct UV writing technology. With varying refractive indices of various drug conc., the characteristics of the biosensor were simulated. The biosensor's sensitivity was determined to be 1606.2 nm/RIU. The limit of detection (LoD) and resolution were specified as 3×10^{-5} RIU and 0.05 nm, respectively [139].

A multilayer polymeric-inorganic composite WG arrangement was used to produce an evanescent field sensor [140]. The low RI polymer layers are covered by layers of a Ta_2O_5 thin film that was produced by sputtering, creating the composite WG structure. According to the results, the polymer-based sensor can detect molecules adhering to surfaces down to a limit of around 100 fg/mm^2 for molecular adsorption detection and an LoD of 3×10^{-7} RIU for RI sensing. The inorganic coating on the polymer layer was discovered to successfully limit water absorption into the WG, which led to stabilized sensor operation in addition to greatly increasing sensitivity. By examining antibody–antigen binding interactions, it was demonstrated that the created sensor can be used in precise molecular detection [140].

For the detection of biomolecules in the lower nano-molar (nM) range, a surface plasmon resonance (SPR) biosensor based on a planar-optical multi-mode polymer WG structure is presented in [141]. With a measuring resolution of 4.3×10^{-3} RIU, the fundamental sensor exhibits a sensitivity of 608 nm/RIU when subjected to variations in RI. C-reactive protein (CRP) was detected in a buffer solution with a response of 0.118 nm/nM by integrating the SPR sensor with an aptamer-functionalized, gold-nanoparticle (AuNP)-enhanced sandwich assay. The biosensor is highly suited for low-cost disposable lab-on-a-chip operations because of the multi-mode polymer WG structure and the straightforward concept. It may also be employed with very straightforward and affordable equipment. The sensor specifically offers the ability for quick and multiplexed identification of various biomarkers on a single integrated technology [141].

There is much interest in polymer-based materials used in photonic circuits, such as benzocyclobutene (BCB), SU8, and PMMA, for label-free, cost-effective biosensing and communications applications [142,143]. It is simple to embed optical components and electronics into polymers [144]. In comparison to low-contrast polymer-based WGs, high-index contrast materials like silicon and silicon nitride give substantial loss inside wall scattering [145,146]. This eliminates any manufacturing limitations and enables the construction of polymer-based WGs with a large footprint in a silicon wafer and minimal side wall scattering loss. These polymer materials may be used in a variety of devices, and by doping impurities, one can adjust the material's optical, thermal, and electrical properties. High sensitivity is provided by an RI-based biosensor using a unique horizontal slot WG structure composed of cost-effective polymer material in an MZI configuration as shown in Figure 6a [147]. The possibility of creating novel hybrid WGs for sensors using silicon wafer-based polymer material has arisen because of the recent need for low-cost point-of-care biosensors. The core of the sensor is made of SU8 material, the outside layer of the sensor is made of PMMA, and the inner layer is made of BCB.

It is suggested and quantitatively proved that a novel evanescent wave biosensor based on the modal interaction between the fundamental mode and the second-order mode is possible [148]. It is feasible to create a device where only the fundamental and second-order modes may propagate, without stimulation of the first-order mode, by considering the characteristics of their symmetry as shown in Figure 6b. Due to the significant contact between the evanescent field and the outer surface as a comparison to prior evanescent wave-based biosensor designs, it is feasible to obtain a high sensitivity response in the biosensor arrangement with this mode selection. The LoD of the device is ~7.34×10^{-7} RIU.

Although polymeric WGs have been suggested as a means of lowering production costs, it has not been feasible to create biosensors with sensitivity levels that are on par with those made available by silicon photonic technology due to the polymeric material's low RI. Therefore, a multimode interferometer has two special features that combine to improve the sensitivity of a modal biosensor interferometer: first, a novel modal interferometer with greater penetration depth by high order mode evanescent tail; and second, a high modal interaction by coupling mode theory optimization. This feature is essential for making lab-on-chip technologies accessible and widely manufactured in underdeveloped parts of the globe [148].

It is the first time that an all-optical plasmonic sensor platform based on integrated planar-optical WG structures in a polymer chip has been published as shown in Figure 6c [149]. The detection of 25-hydroxyvitamin D (25OHD) in human serum samples using an aptamer-based assay was performed to show the sensor system's usefulness for biosensing. The devised assay allowed for the achievement of 25OHD conc. between 0 and 100 nM with a sensitivity of 0.752 pixels/nM. It is possible to simultaneously detect several analytes, including biomarkers, because of the WG structure of the sensor's miniaturization and parallelization capabilities. It is possible to fabricate large-scale, economically priced sensors by integrating the entire optical setup onto a single polymer chip. The proposed concept is particularly appealing for its wider use in lab-on-chip solutions due to the widespread use and accessibility of smartphone electronics [149].

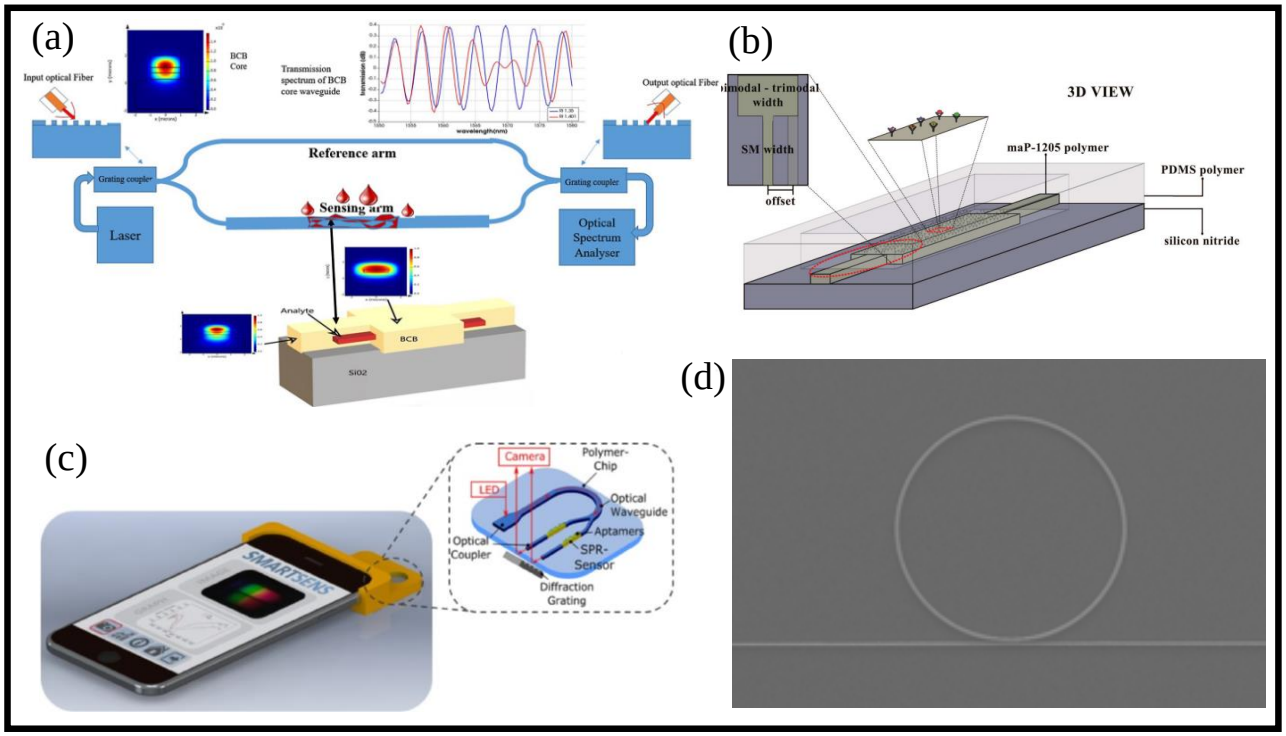


Figure 6. Polymer WG-based biosensors, (**a**) BCB and SU-8 photonic WG in MZI architecture for point-of-care device [147], (**b**) Multimode interferometer [148], (**c**,**d**) SEM image of the polymer WG resonator [150].

Numerous studies are being conducted on optical micro-ring resonators as a possible label-free biosensing technology for use in environmental monitoring and medical diagnostics. The surface mass loading or the change in RI brought on by the presence of analytes in the surrounding media is investigated in these micro-rings using the evanescent fields of the resonant light [3]. It is suggested to use the high-quality SU-8 micro-ring resonators made by NIL for biosensing applications [150]. The SEM image of the ring resonator is shown in Figure 6d. Due to its exceptional optical and mechanical qualities, strong corro-

sion resistance, and high thermal stability, SU-8 polymer has received extensive research in the fields of photonics and microfluidics. Its high level of cross-linking has a special ability to build sidewalls with straight profiles and large aspect ratios. A record-high intrinsic Q-factor of 8.0×10^5 is attained by UV imprinting the device with a transparent polymer mold that was copied from a smooth-sidewall silicon master mold.

4.2. Polymer WG-Based Gas Sensors

For detecting various harmful gases, several optical WG-based techniques have been put forth [151]. These methods may be roughly divided into two subgroups: RI sensing and optical absorption sensing [118,152]. The principle behind RI sensing is to track changes in the analyte's RI, which would affect the output light's frequency or phase. Since each gas has a distinct absorption wavelength, optical absorption spectroscopy-based WG sensors are more selective than RI sensing. The conc. of the gas can be estimated by analyzing the light attenuation that occurs when the light of a certain wavelength flows through the gas [153]. According to the Lambert–Beer Law, increasing the optical path—the distance over which light interacts with the analyte—will lower the LoD [154]. For optical WG sensors, the ambient gas interacts with the WG's evanescent field and serves as its cladding [155].

Beginning in the early 1980s, conducting polymers including polypyrrole (PPy), polyaniline (Pani), polythiophene (PTh), and their derivatives were utilized as the active layers of gas sensors [156]. The sensors built of conducting polymers offer numerous better properties in contrast to most of the widely viable sensors, which are often based on metal oxides and operated at high temperatures. These feathers in particular are guaranteed to be at room temperature and have high sensitivity and rapid reaction times. Conducting polymers are simple to make using chemical or electrochemical methods, and it is simple to change their molecular chain structure via copolymerization or structural derivations. Additionally, conducting polymers have outstanding mechanical qualities that make it simple to fabricate sensors.

The selective and sensitive sensing of harmful greenhouse gases is a significant challenge in the environmental and industrial domains due to the growing emphasis on environmental protection and monitoring [113,118]. Carbon dioxide (CO_2) is one of the principal greenhouse gases that is created in the environment. According to the operating environments and application areas, several specific kinds of CO_2 sensors have been produced during the last few decades. CO_2 sensors can be broadly categorized as electrochemical gas sensors, optical gas sensors, and acoustic gas sensors based on the detecting processes they use [118,157,158]. The choice and design of the sensing material used in a sensing device have a substantial impact on how well the sensor performs since a gas sensor relies on active interaction between the sensing layer and the target gas. Metal oxide, polymers, carbon compounds including carbon nanotubes (CNTs) and graphene, metal–organic frameworks (MOFs), and composites of these materials are the most often employed active materials in CO_2 sensing [159,160]. A flexible CO_2 gas sensor working at room temperature based on CNTs is developed on a low-cost polyimide substrate [159]. Resistive networks are utilized in gas detection to create very uniform CNT thin films using a trustworthy and repeatable transfer technique. When the ambient CO_2 gas conc. was 800 ppm, the flexible gas sensor had a high sensitivity of 2.23%.

MOF-based optical gas sensors, which focus primarily on light–gas interaction within a thin MOF layer, are preferable due to their properties of minimal drift, high gas selectivity to other gases—pertinent for the optical gas sensing part—and the high porosity, large surface area, and tailor-made pore sizes related for the optical gas sensing part. Metal–organic frameworks are porous crystalline solids that are put together by the coordination of inorganic building units by organic linker molecules. Because MOFs' pores may be replaced with different substances, they are appealing for use in a variety of applications, including gas storage, gas separation, catalysis, and sensing.

Air and hydrogen mixes may catch fire easily. Therefore, hydrogen sensors are crucial for quick leak identification during handling. Existing solutions, nevertheless, fall short of the high-performance standards established by stakeholders, and deactivation brought on by poisoning—such as that caused by carbon monoxide—remains a significant issue. In a plasmonic metal–polymer hybrid nanomaterial idea, deactivation resistance is supplied by a specially designed tandem polymer membrane, while the polymer coating lowers the apparent activation energy for hydrogen transport into and out of the plasmonic nanoparticles [161]. This provides subsecond sensor response times in conjunction with the optimum volume-to-surface ratio of the signal transducer given exclusively by nanoparticles. In addition, sensor LoD is improved, hydrogen sorption hysteresis is reduced, and sensor operation in challenging chemical conditions is made possible without long-term deactivation symptoms [161].

The development of affordable PCB-integrated optical WG sensors is shown using a unique platform [162]. The sensor design depends on the utilization of multimode polymer WGs that can be created directly on common PCBs and chemical dyes that are readily accessible in the market, allowing the assembly of all crucial sensing elements (electronic, photonic, and chemical) on low-cost substrates. Furthermore, it uses WG arrays functionalized with various chemical dyes to permit the detection of many analytes from a single device. The devices may be made using PCB manufacturing techniques that are standard practice, such as pick-and-place assembly and solder-reflow operations. An FR4 substrate is used to construct an ammonia gas sensor that is PCB integrated as a proof of concept. The sensor's functionality depends on the way ammonia molecules affect the optical transmission properties of chemically functionalized optical WGs. In addition to the basic modeling and characterization investigations, the manufacturing and assembly of the sensor unit are discussed. At normal temperatures, the device achieves a sensitivity of around 30 ppm and a linear response of up to 600 ppm. Finally, principal-component assessment is used to show how it is possible to identify numerous analytes from a single device [162].

For the detection and sensing of CO_2, a cheap gas sensor based on planar polymer optical WGs with an embedded zeolite imidazole framework-8 (ZIF-8) thin film is presented [68]. The PMMA planar optical WGs are formed by hot embossing, which makes them flexible and economical. A simple solution approach is used to evenly produce thin ZIF-8 films on the surface of WGs, which is essential for the envisioned mass manufacturing of metal–organic framework-based sensing devices. The microscope image of the WG without MOF film and with MOF film is shown in Figure 7a,b, respectively.

Figure 7c depicts the recording of optical signal transmission out of the MOF-coated WG with a gas switching time interval of t = 1 min. Several cycles were repeated. The alternate purging of N_2 and CO_2 caused the transmission signal to shift frequently and reproducibly. When CO_2 was released into the gas cell, the transmission rapidly fell and maintained a largely constant level. The repeated cycle tests provide additional evidence of the proposed MOF-based polymer WGs' resilience and effectiveness as sensors. A further experiment with t = 30 s was carried out to test the optical response of the planar WG sensor to CO_2 exposure during shorter gas changeover times. Figure 7d depicts the outcome. The optical signal leaving the WG here also changes regularly due to the alternate purging of N_2 and CO_2. Additionally, it can be shown that the short gas switching time results in a high-power level when N_2 is purged that lacks a clear steady state. The time from the response's beginning to 90% of its maximum in a steady state is referred to as the adsorption and desorption times. The MOF-coated PMMA WG used in this study exhibits CO_2 adsorption and desorption times of approximately 6 s and 16 s, respectively, as shown in Figure 7e. These findings show that the diffusion of gases into the MOF sensing layer from the surrounding medium occurs at a very high rate. According to experimental findings, the developed optical elements have good reversibility of the gas molecules' adsorption and desorption, a sensitivity of 2.5 μW/5 vol% toward CO_2 [68].

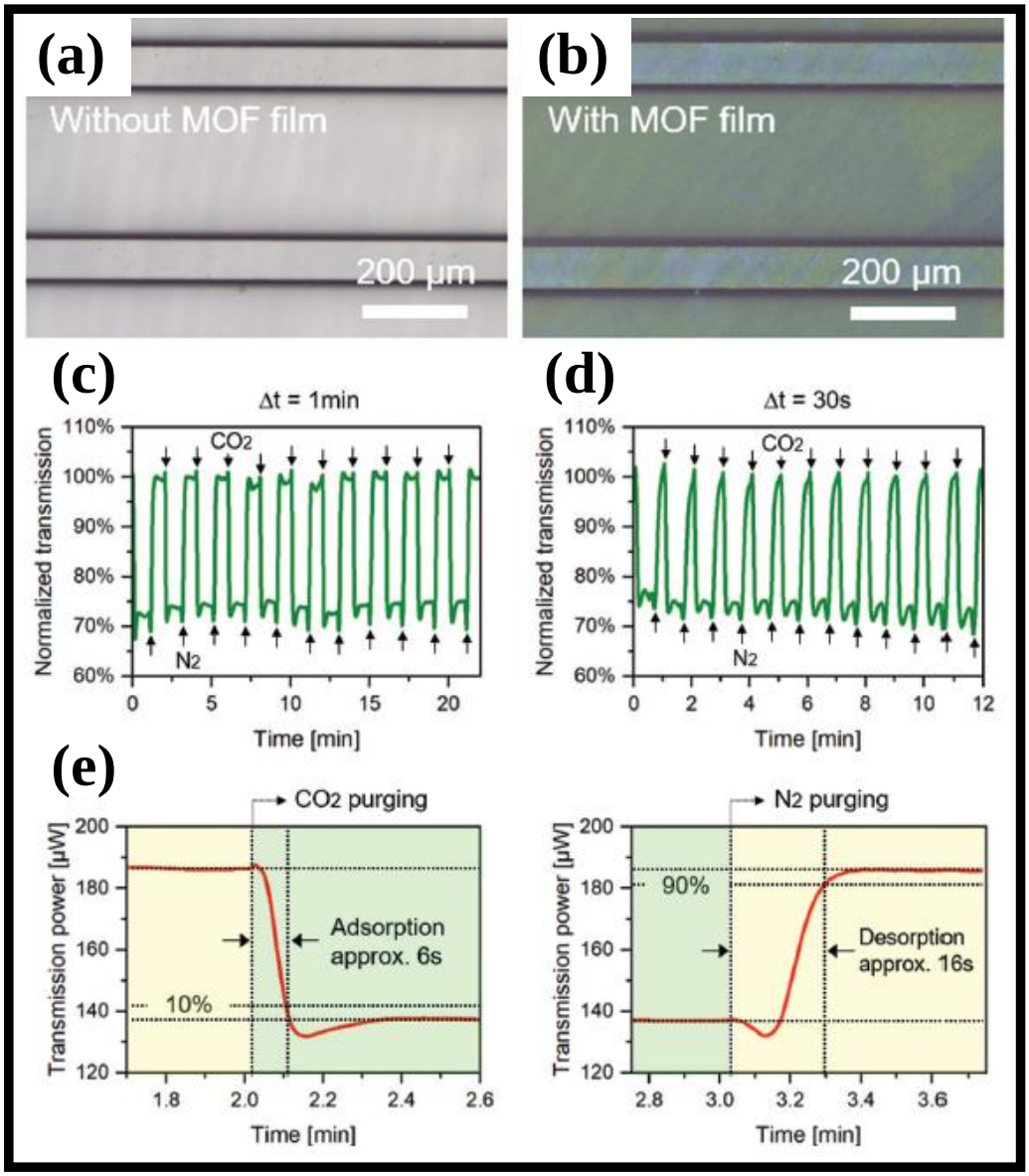


Figure 7. Microscope images of (**a**) uncoated [68], (**b**) ZIF-8 coated WG [68], (**c**) response of the MOF-coated WG to CO_2 with gas switching time intervals of 1 min [68], (**d**) response of the MOF-coated WG to CO_2 with gas switching time intervals of the 30 s [68], and (**e**) adsorption and desorption time of MOF-coated WG sensor [68].

4.3. Polymer WG-Based Temperature Sensors

In several industries and applications, including healthcare, consumer electronics, transportation, and aerospace, temperature sensors are crucial [163,164]. To meet the expanding demands for automation in production and monitoring, there is an expanding market for temperature sensors that are high-performing, trustworthy, and affordable [165]. Such sensors are increasingly being included in materials (such as composites) during the manufacturing process. Conventional electronic-based temperature sensors are unsuitable for several tasks because of their sensitivity to electromagnetic interference [166].

Optical WGs on a planar substrate are an intriguing solution to fibers for sensing since they may incorporate splitters, optoelectronic components, or even whole Bragg grating interrogation systems [167,168]. Comparatively to single fiber sensors, the use of planar foils makes it easier to position and align the sensors during integration. Due to the wide range of materials that are readily accessible, each with unique features and optimized for certain manufacturing methods, Bragg grating-based sensors in polymer WGs are becoming

more and more popular in several applications [169–175]. Because of its high thermo-optic coefficient, superior thermal stability, and relatively low absorption loss from visible to telecom wavelengths, Ormocer, an inorganic-organic hybrid polymer, is an excellent option to be utilized in the implementation of a Bragg grating-based temperature sensor. Additionally, the material is economical, simple to utilize, and risk-free to handle without specific safeguards. However, due to its oxygen inhibition and liquid condition during UV exposure, traditional contact mask lithography makes it challenging to define nanometer-scale WG features. An equivalent has been imprinting-based technology; however, because of the rather thick residual layer, the reported structures made with this approach are inverted-rib WGs [176]. To create a highly sensitive Ormocer-based WG Bragg grating temperature sensor, a novel capillary filling-based duplication technique is suggested [177]. A series of polymer WGs imprinted with a wide area grating is patterned on top of an under-cladding layer to create the sensor, which has a sensitivity of −249 pm/°C at ambient temperature and a working wavelength of 1530 nm [177].

The use of switchable molecular compounds in a polymer WG-based temperature sensor system is described in [178]. A maskless lithographic optical system is used to manufacture the polymer WG cladding, and hot embossing equipment is used to copy it onto polymer material (for instance polymethyl methacrylate (PMMA)). The substance used to monitor changes in outside temperature is a molecular combination of iron, amino, and triazole. A mixture of core material (NOA68) is used to fill the WG's core for this purpose, and doctor blading and UV curing are used to solidify the molecular complex. In the low-spin state, two distinct absorption bands are present in the molecular complex's UV/VIS light spectrum. A spin-crossover transition takes place when the temperature gets close to room temperature, which causes the molecular complex to go from violet pink to white (or spectral characteristics). With a hysteresis width of around 12 °C and a sensitivity of 0.08 mW/°C, the measurement of optical power transmitted through the WG as a function of temperature displays a memory effect. In situations where electromagnetic interference might skew the results, this permits optical rather than electrical temperature detection [178].

A polymer WG incorporated in an optical fiber micro-cavity-based MZI was presented [179]. Femtosecond laser micromachining, fiber splicing, and single-mode fibers were used to create the micro-cavity with two symmetric apertures. The 70 µm long polymer WG was then fabricated using the two-photon polymerization manufacturing technique and incorporated into the micro-cavity. A complete interference spectrum and over 25 dB of fringe visibility were displayed by the MZI. The suggested MZI's temperature sensitivity exceeded 447 pm/°C because of the strong thermo-optical coefficient of the polymer material. Due to its flawless linearity (99.7%) and persistence, it may be utilized as a trustworthy temperature sensor [179].

It is suggested to use an asymmetric MZI with varying widths in the two interferometer arms as the foundation for an ultra-sensitive polymeric WG temperature sensor [180]. The device's sensitivity was improved by using a polymer with a higher thermo-optic coefficient (TOC). The effect of the two arms' distinct widths and the cladding materials' various TOCs on the sensor's sensitivity was investigated and experimentally proven. The devices were created by combining a straightforward all-wet etching method with conventional photolithography. The sensitivity of the WG temperature sensor was found to be 30.8 nm/°C when the cladding material Norland optical adhesive 73 (NOA 73) and the width difference of 6.5 µm were used. Additionally, the lowest temperature resolution was almost 0.97×10^{-3} °C. The sensor has the specific benefits of high sensitivity, high resolution, simple manufacture, low cost, and biological compatibility, making it potentially useful for temperature detection of organisms, molecular analysis, and biotechnology [180].

With the use of bottom metal printing technology, multimodal responsive optical WG sensors that make use of a stable cross-linking gel polymer electrolyte have been successfully created [181]. Figure 8a depicts the prototype optical WG multimodal sensor's schematic structure diagram. First, Si substrates with SiO_2 buffer layers are used to fabricate

metal thermo-inducting electrode designs. Spin-coating and UV curing are used to cure a gel polymer electrolyte that was self-created as a sensing WG material on metal electrodes. By using the bottom metal printing process, the MMI WG sensing structure is directly defined through electrode areas. The lift-off technique is used to detach the polymer films off the thermo-inducting electrodes' pads on both sides. Next, a printed circuit board (PCB) is attached to the overall sensing WG chip using adhesive. On either side of the chip, two further PCBs are connected. Copper and aluminum metal electrode pads on two different PCBs with holes that are aligned to them might make a thermo-inducting contact. Figure 8b provides the packed chip's complete model diagram. Figure 8c,d show the measurement systems of the multimodal photonic chip for temperature and humidity sensing applications, respectively [181].

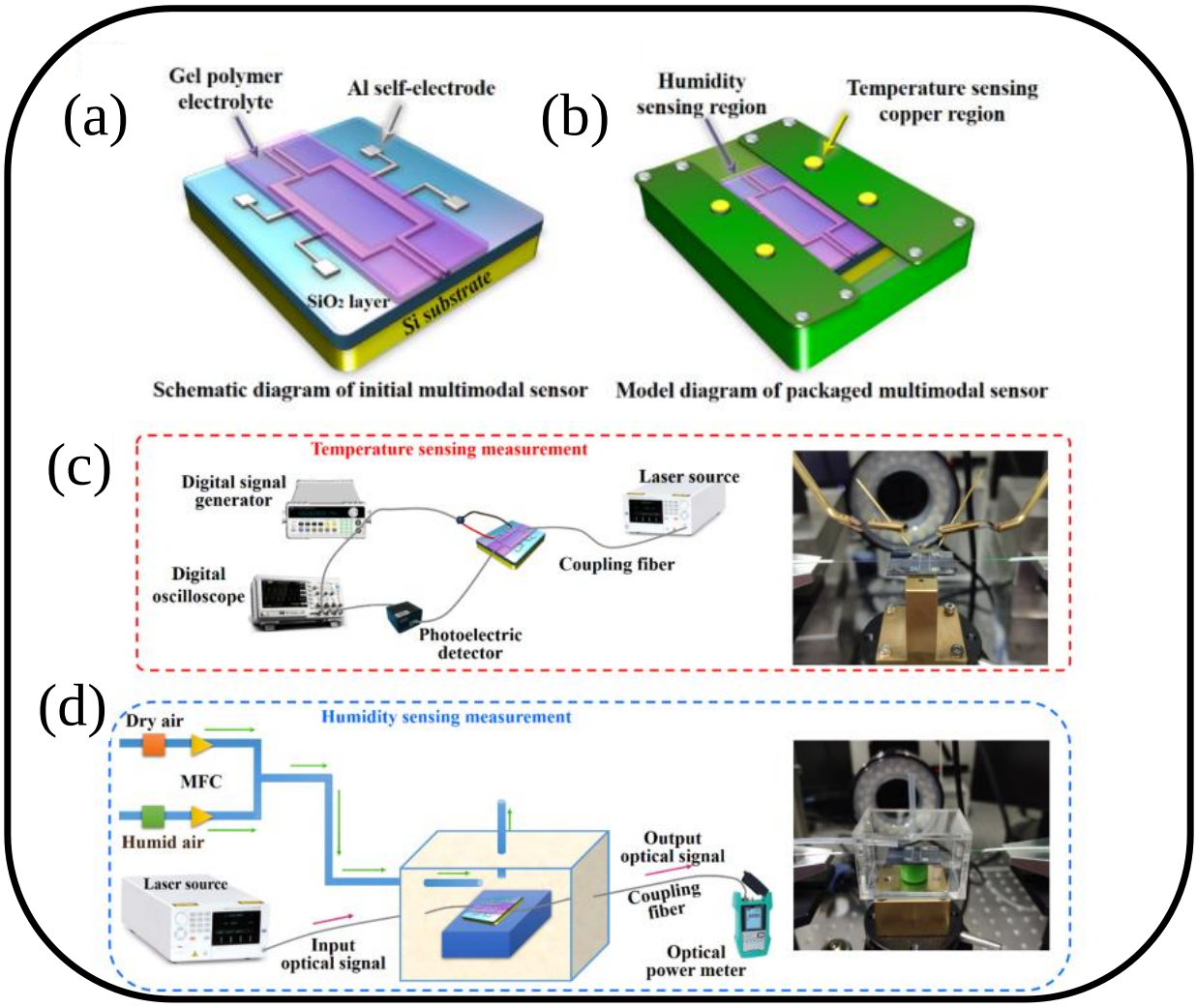


Figure 8. Graphical illustration of (**a**) the prototype of optical WG multimodal sensor [181], (**b**) packaged photonic multimodal sensor [181], (**c**) measuring systems of the sensor for temperature [181], and (**d**) measuring systems of the sensor for humidity [181].

It is simulated to characterize temperature and humidity sensing using a polymer electrolyte. Considering the study of ion relaxation dynamics, the multimodal responsive features of the photonic chip are established: optical attenuation and phase variables for temperature and humidity sensing, respectively. The device's temperature and humidity sensitivities were measured at 0.5 rad/°C and 1.14 dB/% RH, respectively, in the monitoring temperature (36.0–38.0 °C) and relative humidity (45%–65%) ranges. The multifunctional sensor's quick reaction times may be calculated to be 4.21 ms and 1.32 s, for temperature

and humidity, respectively. This study offers a workable plan for the development and use of temperature and humidity sensors in possible medical procedures [181].

4.4. Polymer WG-Based Mechanical Sensors

Polymer WG-based mechanical sensors are devices that use the optical properties of a polymer WG to detect mechanical changes. When the WG is deformed due to mechanical stress or strain, the refractive index of the material changes, which alters the way that light propagates through it. This change in the optical properties of the WG can be measured and used to detect the presence and magnitude of the mechanical stress or strain. Polymer WG mechanical sensors have a number of potential applications, including in structural health monitoring, biomedical sensing, and environmental monitoring. There are different types of polymer WG-based mechanical sensors, including cantilever-based sensors, micro-ring resonator sensors, and Mach–Zehnder interferometer sensors. Each of these sensors has its own advantages and disadvantages, and the choice of sensor depends on the specific application requirements.

Optical sensors with low residual stress, straightforward manufacturing, and low cost have been created employing polymer-based WG systems. In general, the mechanical characteristics of polymers may be described in a manner quite similar to those of metals or other common crystalline materials. This is especially true for elastic moduli and other classes of strength measures like yield and tensile strengths. A wide range of biomedical applications in sensing, diagnostics, and phototherapy have demonstrated considerable potential for biocompatible polymeric optical WGs with soft and flexible mechanical features [182]. Today, transparent touch-sensitive panels for portable devices like smartphones and tablet computers are commonly used. These panels have become more functional and versatile, enabling multipoint touch interaction in addition to single point touch, which is a growing trend in touch sensing in electronic devices. Besides contact detection, pressure-based touchscreen interaction increases usability. For instance, a touch-sensitive keyboard performs better when pressing the keys. Recently, flexible or even stretchy touch sensors were developed so they can work with flexible screens [166].

A high sensitivity of 8.2 ppm/Pa has been established for an optomechanical pressure sensor employing polymer multimode interference (MMI) couplers [183]. It has been established that a polymer WG sensor with a symmetric multilayer design may be used to detect low humidity conc. [184]. When water molecules diffuse into the polymer WG, the sensor records the resultant optical phase shifts. It is possible to reach a sensitivity of several parts per million for humidity levels. Additionally, the sensor provides the absolute sign of the movement of the generated interference fringes, which makes it simple to identify trends in the index (increase or reduction) in the sensing layer. This work shows a very promising future for the development of a small, disposable optical sensor with a cheap cost for humidity sensing applications [184].

Stretchable polymeric optical WGs have also been researched for wearable body temperature readings in addition to mechanical sensing [185]. One of the most important physiological indicators that accurately identifies stages of health is body temperature. The reading of wearable temperature sensors should be resistant to body motions and independent of mechanical deformation for continuous and long-term temperature monitoring. Utilizing PDMS optical fibers that have integrated upconversion nanoparticles, a unique stretchable optical temperature sensor that can maintain its sensing capability despite massive strain deformations (up to 80%) has been produced [185].

The main criteria, such as thin-film design, localized force sensing, multiple-point identification, and bending resilience, as well as a quick response for a tactile sensor functioning on curved surfaces, are satisfied by a polymer WG-based transparent and flexible force sensor array [186]. A contact force with a location at 27 different spots is detected by the force sensor array separately. The sensor array is elastic, thin (total thickness: 150 μm), as well as very transparent (transmittance: up to 90%). The force sensor can detect contact forces at one or more points with a quick response (response delay: 10 ms), high

replicability (Pearson correlation coefficient: as high as 0.994, hysteresis: as low as 6.7%), high sensitivity (as high as 16% N^{-1}), and high bendability (10.8% sensitivity degradation at a bending radius of 1.5 mm), all without utilizing any electronic components. Without noticeably degrading its function, the sensor can detect pressure on curved objects as well as soft ones like the human body. For detecting dynamic contact forces on different surfaces, the force sensor could be employed in a variety of applications [186]. The fabrication process of the sensor is shown in Figure 9a. The SEM image and an optical microscope image of the sensing area is shown in Figure 9b,c, respectively. Despite its multilayered configuration, the WG layer exhibits excellent optical transparency of 90% in the range of 550–1000 nm, allowing removal from the stiff substrate without mechanical damage as shown in Figure 9d. Due to the soft nature of the materials utilized for both the clad and core, the WG-based thin force sensor is mechanically resilient to bending, twisting, or folding and is capable of close contact with a forearm with great transparency and flexibility as shown in Figure 9e–g [186].

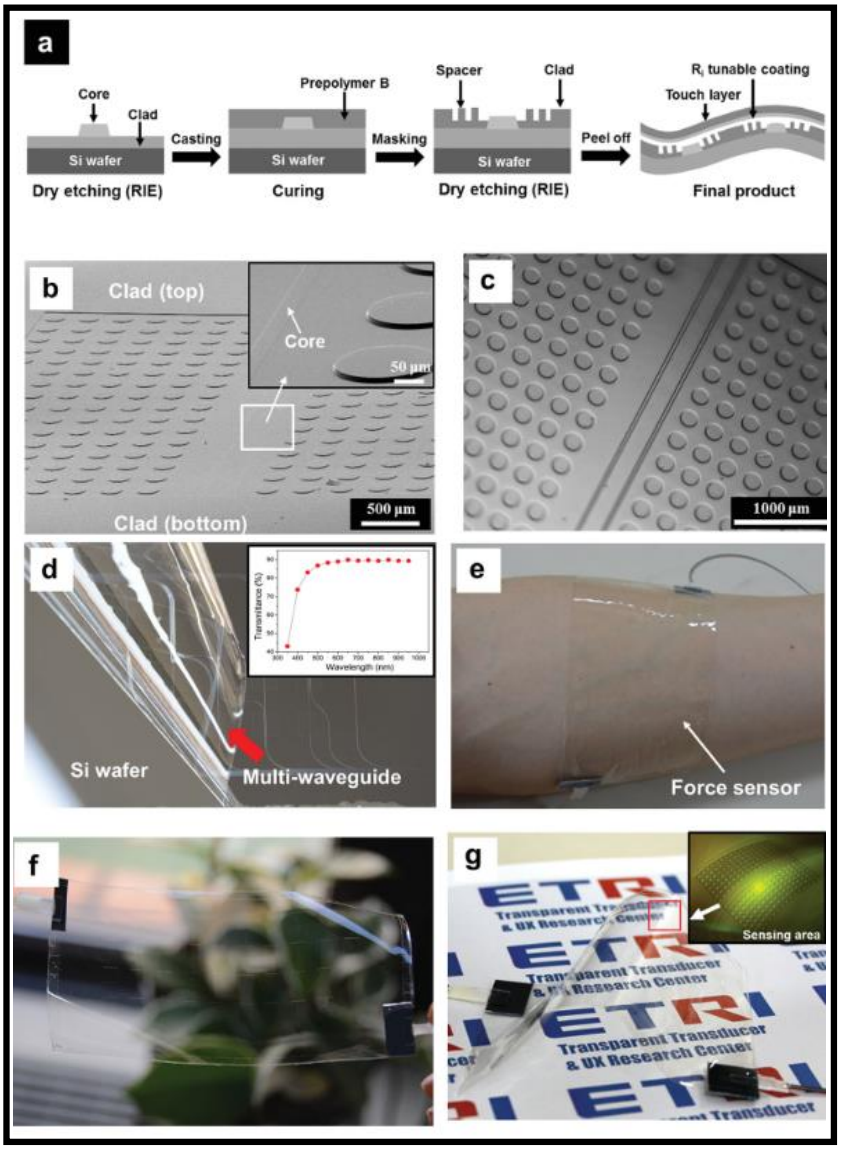


Figure 9. (**a**) Fabrication process of a WG-based sensor, (**b**) SEM image, and (**c**) optical microscope image of a WG [186], (**d**) an image showing the construction of the waveguide layer being peeled from a Si wafer [186], (**e**) photo demonstrating the close proximity of a thin-film sensor to a forearm [186], (**f**) the transparency of the sensor [186], and (**g**) a photograph and an optical microscope image (inset) of a force sensor deformed by mechanical bending [186].

A photopolymerizable resin solution that self-writes a strain sensor WG is described as an experimental demonstration [187]. The sensor is created between two multi-mode optical fibers using ultraviolet (UV) light waves, and it functions as a sensor by examining the power that is passed through the WG in the infrared (IR) wavelength range. Following sensor failure brought on by loading, the WG uses UV resin to re-bridge the gap between the two optical fibers. Measurements reveal similarities in the responses of the original and self-repaired sensors under strain [187].

Due to the weak mechanical strengths of most synthetic hydrogels, hydrogel optical WGs are frequently brittle and unstable when subjected to strain deformations. Due to the possibility of WG structural damage from body/tissue movement, this property limits their use in wearable or implanted sensors. For the creation of optical fibers, hybrid ionic/covalent hydrogels with high stretchability and toughness were used to produce great deformability and robustness. Hybrid alginate–polyacrylamide hydrogels have been molded and dip-coated to create robust, stretchable hydrogel optical fibers with an overall step-index profile [188]. Table 2 presents the recently proposed polymer WGs employed for biosensing, gas sensing, temperature sensing, and mechanical sensing.

Table 2. Recently proposed polymer WG-based biosensors, gas sensors, temperature sensors, and mechanical sensors.

Polymer	Sensor Design	Application	Temperature Range (°C)	Sensitivity	Fabrication Method	Numerical/Experimental	Ref.
NOA 73	MZI	Temperature	-	30.8 nm/°C	Wet etching	Experimental	[180]
Gel polymer	MZI	Temperature	36–38	0.5π rad/°C	Bottom metal-printing	Experimental	[181]
NOA 73	MZI	-Temperature	25–75	−431 pm/°C	CMOS	Experimental	[189]
PDMS	PhC	Temperature	10–90	0.109 nm/°C	-	Numerical	[82]
PMMA	BG	Temperature	−10–70	−48.6 pm/°C	Direct laser writing	Experimental	[190]
NOA68	Planar WG	Temperature	18–35	0.08 mW/°C	Hot embossing	Experimental	[178]
COC	BG	Temperature	30–160	−7.3 pm/K	Single writing step	Experimental	[191]
PDMS	Metasurface	Temperature	30–60	−0.18 nm/°C	-	Numerical	[192]
PDMS	FPI-AWG	Temperature	30–40	−0.854 dB/°C	-	Experimental	[193]
SU-8	Trimodal WG interferometer	Temperature	22–27	0.0586 dB/°C	Direct laser writing	Experimental	[194]
Ormocer	BG	Temperature	20–110	−150 pm/°C	Imprinting	Experimental	[195]
ZIF-8	Planar WG	CO_2	-	2.5 μW/5 vol%	Hot embossing	Experimental	[68]
PHMB	Modified BG	CO_2	-	226 pm/ppm	-	Numerical	[196]
-	Planar WG	CO	-	-	NIL	Experimental	[197]
PMMA	Photonic crystal nanocavity		-	287 ppb/$\sqrt{\text{Hz}}$	EBL	Experimental	[198]
PHMB	Plasmonic WG	CO_2	-	135.95 pm/ppm		Numerical	[199]
PHMB	Metasurface	CO_2	-	17.3 pm/ppm		Numerical	[98]
BCB and SU8	MZI	Biosensing	-	19,280 nm/RIU and 16,500 nm/RIU	N/A	Numerical	[147]
FSU-8 and PMMA	BG	Drug conc.	-	1606.2 nm/RIU	Direct UV writing	Experimental	[139]
PMMA and NOA 63	Planar WG structure	Vitamin D	-	0.752 pixel/nM	Hot embossing and doctor blading	Experimental	[149]
PMMA and NOA 63	Planar optical multi-mode WG	C-reactive protein	-	608.6 nm/RIU	Hot embossing and doctor blading	Experimental	[141]
PEI, PSS and PAH	Phase-shifted BG	NaCl	-	579.2 nm/RIU	CMOS	Experimental	[200]
Ormocore	Micro-ring	Biosensing	-	-	Soft UV NIL	Experimental	[201]

Table 2. *Cont.*

Polymer	Sensor Design	Application	Temperature Range (°C)	Sensitivity	Fabrication Method	Numerical/Experimental	Ref.
Ma-P 1205	Trimodal interferometer	Biosensing	-	2050 2π/RIU	-	Numerical	[109]
SU8/PMATRIFE	Ring resonator and MZI	Glucose	-	17,558 nm/RIU	CMOS	Experimental	[202]
Ormocore	MZI	Biosensing	-	10^4 nm/RIU	-	Numerical	[203]
PEI-B	MZI	STA-biotin	-	-	Inkjet printing	Experimental	[204]
PMMA	Polymer optical fiber	Breath and heartbeat	-	Error compared with reference: 1 cpm (breath) 4 bpm (heartbeat)	-	Experimental	[205]
PMMA	Polymer optical fiber	Smart textile: Bending, compression	-	-	Melt-spinning	Experimental	[206]
PDMS	Polymer optical fiber	Smart textile: Bending, compression	-	-	Moulding	Experimental	[206]
PMMA	Polymer optical fiber BG	Pressure	-	Up to 71.9 ± 0.3 µm/MPa	-	Experimental	[207]
-	Optical fiber-based polymer Fabry–Perot interferometer	Gas pressure	-	3.959 nm/MPa	3D-printed	Experimental	[208]

5. Conclusions and Outlook

The global sensor market is rapidly expanding due to the establishment and expansion of new applications, such as medical devices that use noninvasive optical sensors and environmental monitoring, which is gaining prominence due to an increase in the demand for both indoor and outdoor air quality measurements. Several planar WG systems have appeared in the last 10 years. They are characterized by the materials systems employed and their distinct qualities, which confer restrictions and benefits on each. For a very long period, most of these platforms were developed primarily to support applications from the telecommunications industry. Because of the wide variety of chemical structures and inherent features that polymers may take on, they have long been regarded in the engineering community as exceptional materials systems. However, due to their ease of manufacture in recent years, polymer optics have drawn increased interest.

Polymer WGs can be designed with small core diameters, which increases the sensitivity of the sensor to changes in the environment. These WGs are typically less expensive to manufacture than other types of optical fibers, making them an attractive option for cost-sensitive applications and can be bent and shaped into a variety of configurations, which allows for easy integration into various applications and environments. These WGs are typically lighter than other types of optical fibers, which makes them ideal for portable and mobile applications. They are typically more durable and resistant to damage than other types of optical fibers, which makes them suitable for use in harsh environments, and can be easily integrated with other optical components, such as lenses, detectors, and electronics, which makes them a flexible and versatile option for a variety of applications. Keeping in mind the potential of polymer WG sensors, four main sensing applications which include biosensing, gas sensing, temperature sensing, and mechanical sensing are reviewed.

Nevertheless, polymer sensors are not significantly inferior to sensors based on integrated photonics or classical FBG sensors. We have previously mentioned that the sensitivity of FBGs based on polymer fibers can exceed 1600 nm/RIU. At the same time, the sensitivity of refractive index sensors based on inorganic FBGs varies in different sources. Thus, in [209], a sensitivity of 1210.49 nm/RIU is shown. In [210], the sensitivity of a phase-shifting FBG is 463.7953 nm/RIU. At the same time, in [211], the sensitivity varies from 1008 dB/RIU for the high RI range to 8160 dB/RIU for the low RI range; however, a high sensitivity value is achieved by optimizing the cladding diameter, which is a techno-

logically complex process. The sensitivity of sensors based on integrated photonics devices is often inferior to polymer sensors. In this case, the advantage of integrated photonics is the ability to implement the entire sensor system (including the interrogator) on a single chip [212,213].

A wide range of polymeric materials and methods of their use suggests expanding areas of application and production methods. For example, [214] shows the possibility of creating polymer fibers based on natural cellulose, transparent in the wavelength range from 500 nm to 4000 nm. The work [215] shows broad prospects for the creation of MWIR-range (Mid-Wavelength Infrared) devices, opening up with the use of organically modified chalcogenides (ORMOCHALC). The work shows the prospects for the creation of polymer optical fibers based on multi-materials (PMMA and Polycaprolactone (PCL)) for use in sensors. Finally, work [216] demonstrates the possibility of increasing the sensitivity of the SPR sensor when using meta-dielectric materials up to 1700 nm/RIU. Thus, the development and application of polymer-based sensors is a rapidly developing field of knowledge with a wide range of applications and prospects.

Author Contributions: Conceptualization, M.A.B. and G.S.V.; methodology, S.N.K., M.A.B. and N.L.K.; software, S.N.K., M.A.B. and N.L.K.; validation, S.N.K., M.A.B. and N.L.K.; formal analysis, G.S.V., S.N.K., M.A.B. and N.L.K.; investigation, S.N.K., E.P.G., M.A.B. and N.L.K.; resources, S.N.K., M.A.B. and N.L.K.; data curation, R.V.K., S.N.K., M.A.B. and N.L.K.; writing—original draft preparation, S.N.K., M.A.B. and N.L.K.; writing—review and editing, S.N.K., E.P.G., R.V.K., G.S.V., M.A.B. and N.L.K.; visualization, S.N.K., M.A.B. and N.L.K.; supervision, S.N.K., M.A.B. and N.L.K.; project administration, S.N.K., E.P.G., M.A.B. and N.L.K.; funding acquisition, S.N.K., M.A.B. and N.L.K. All authors have read and agreed to the published version of the manuscript.

Funding: The research was supported by the Ministry of Science and Higher Education of the Russian Federation in the financing of new laboratories under the guidance of young scientists within the framework of the national Project "Science and Universities" (project FSSS-2021-0016) in the part of sensors' applications and under the FSRC "Crystallography and Photonics" of the Russian Academy of Sciences (the state task No. 007-GZ/Ch3363/26) in the part of sensors' specifications, and by the Ministry of Science and Higher Education of the Russian Federation within the state assignment for the UUST (agreement No. 075-03-2021-014) and conducted in the research laboratory "Sensor systems based on integrated photonics devices" of the Eurasian Scientific and Educational Center in the part of photonics integrated-based sensors' analysis.

Acknowledgments: We acknowledge the equal contribution of all the authors in the completion of this work.

Conflicts of Interest: The authors declare no conflict of interest.

Abbreviations

Waveguide = WG; Limit of detection = LoD; Polymethyl methacrylate = PMMA; Polydimethylsiloxane = PDMS; Surface plasmon resonance = SPR; Mach-Zehnder interferometer = MZI; Polyethyleninmine = PEI; Polystyrene sulfonate (PSS); Polyallylamine hydrochloride = PAH; Polyvinylpyrrolidone = PVP; Cyclic olefin copolymer = COC; Polyhexamethylene biguanide = PHMB; Polypyrrole = PPy; Polyaniline = Pani; Polythiophene = PTh; Refractive index = RI.

References

1. Paquet, C.; Kumacheva, E. Nanostructured polymers for photonics. *Materialstoday* **2008**, *11*, 48–56. [CrossRef]
2. Khan, M.; Rahlves, M.; Lachmayer, R.; Roth, B. Low-cost fabrication of polymer based micro-optical devices for application in illumination, sensing, and optical interconnects. In Proceedings of the Conference on Lasers and Electro-Optics Europe and European Quantum Electronics Conference, Munich, Germany, 23–27 June 2019.
3. Butt, M.A.; Khonina, S.N.; Kazanskiy, N.L. A highly sensitive design of subwavelength grating double-slot waveguide microring resonator. *Laser Phys. Lett.* **2020**, *17*, 076201. [CrossRef]
4. Butt, M.; Khonina, S.; Kazanskiy, N. Optical elements based on silicon photonics. *Comput. Opt.* **2019**, *43*, 1079–1083. [CrossRef]

5. Butt, M.A.; Kozlova, E.S. Multiport optical power splitter design based on coupled-mode theory. *J. Phys. Conf. Ser.* **2019**, *1368*, 022006. [CrossRef]
6. Butt, M.A.; Kozlova, E.S.; Khonina, S.N. Conditions of a single-mode rib channel waveguide based on dielectric TiO_2/SiO_2. *Comput. Opt.* **2017**, *41*, 494–498. [CrossRef]
7. Ma, H.; Jen, A.-Y.; Dalton, L. Polymer-based optical waveguides: Materials, processing, and devices. *Adv. Mater.* **2002**, *14*, 1339–1365. [CrossRef]
8. Wolfer, T.; Bollgruen, P.; Mager, D.; Overmeyer, L.; Korvink, J. Flexographic and inkjet printing of polymer optical waveguides for fully integrated sensor systems. *Procedia Technol.* **2014**, *15*, 521–529. [CrossRef]
9. Han, T.; Madden, S.; Zhang, M.; Charters, R.; Luther-Davies, B. Low loss high index contrast nanoimprinted polysiloxane waveguides. *Opt. Express* **2009**, *17*, 2623–2630. [CrossRef]
10. Hiltunen, J.; Kokkonen, A.; Puustinen, J.; Hiltunen, M.; Lappalainen, J. UV-imprinted single-mode waveguides with low loss at visible wavelength. *IEEE Photonics Technol. Lett.* **2013**, *25*, 996–998. [CrossRef]
11. Wang, S.; Vaidyanathan, V.; Borden, B. Polymer optical channel waveguide components fabricated by using a laser direct writing system. *J. App. Sci. Eng. Technol.* **2009**, *3*, 47–52.
12. Rezem, M.; Gunther, A.; Rahlves, M.; Roth, B.; Reithmeier, E. Hot embossing of polymer optical waveguides for sensing applications. *Procedia Technol.* **2014**, *15*, 514–520. [CrossRef]
13. Butt, M. Thin-film coating methods: A successful marriage of high-quality and cost-effectiveness—A brief exploration. *Coatings* **2022**, *12*, 1115. [CrossRef]
14. Wang, H.; Liu, Y.; Jiang, M.; Chen, C.; Wang, X.; Wang, F.; Zhang, D.; Yi, Y. Three dimensional polymer waveguide using hybrid lithography. *Appl. Opt.* **2015**, *54*, 8412–8416. [CrossRef] [PubMed]
15. Dangel, R.; Hofrichter, J.; Horst, F.; Jubin, D.; Porta, A.; Meier, N.; Soganci, I.; Weiss, J.; Offrein, B. Polymer waveguides for electro-optical integration in data centers and high-performance computers. *Opt. Express* **2015**, *23*, 4736–4750. [CrossRef] [PubMed]
16. Marin, Y.; Nannipieri, T.; Oton, C.; Pasquale, F. Current status and future trends of photonic-integrated FBG interrogators. *J. Light. Technol.* **2018**, *36*, 946–953. [CrossRef]
17. Lin, H.; Luo, Z.; Gu, T.; Kimerling, L.; Wada, K.; Agarwal, A.; Hu, J. Mid-infrared integrated photonics on silicon:A perspective. *Nanophotonics* **2017**, *7*, 393–420. [CrossRef]
18. Sharma, T.; Wang, J.; Kaushik, B.; Cheng, Z.; Kumar, R.; Wei, Z.; Li, X. Review of Recent Progress on Silicon Nitride-Based Photonic Integrated Circuits. *IEEE Access* **2020**, *8*, 195436–195446. [CrossRef]
19. Wang, R.; Vasiliev, A.; Muneeb, M.; Malik, A.; Sprengel, S.; Boehm, G.; Amann, M.-C.; Simonyte, I.; Vizbaras, A.; Vizbaras, K. III-V-on-silicon photonic integrated circuits for spectroscopic sensing in the 2–4 mm wavelength range. *Sensors* **2017**, *17*, 1788. [CrossRef]
20. Prajzler, V.; Jasek, P.; Nekvindova, P. Inorganic–organic hybrid polymer optical planar waveguides for micro-opto-electro-mechanical systems (MOEMS). *Microsyst. Technol.* **2019**, *25*, 2249–2258. [CrossRef]
21. Ibrahim, N.; Riduwan, M.; Rusli, A. Synthesis of Siloxane-polyimide Copolymer with Low Birefringence and Low Loss for Optical Waveguide. *J. Phys. Sci.* **2019**, *30*, 103–113. [CrossRef]
22. Bahadori, M.; Nikdast, M.; Cheng, Q.; Bergman, K. Universal design of waveguide bends in silicon-on-insulator photonics platform. *J. Light. Technol.* **2019**, *37*, 3044–3054. [CrossRef]
23. Sun, X.; Dai, D.; Thylen, L.; Wosinski, L. High-Sensitivity Liquid Refractive-Index Sensor Based on a Mach-Zehnder Interferometer with a Double-Slot Hybrid Plasmonic Waveguide. *Opt. Express* **2015**, *23*, 25688. [CrossRef] [PubMed]
24. Huang, W.; Luo, Y.; Zhang, W.; Li, C.; Li, L.; Yang, Z.; Xu, P. High-sensitivity refractive index sensor based on Ge-Sb-Se chalcogenide microring resonator. *Infrared Phys. Technol.* **2021**, *116*, 103792. [CrossRef]
25. Wu, N.; Xia, L. Side-Mode Suppressed Filter Based on Anangular Grating-Subwavelength Grating Microring Resonator with High Flexibility in Wavelength Design. *Appl. Opt.* **2019**, *58*, 7174. [CrossRef] [PubMed]
26. Xie, W.; Komljenovic, T.; Huang, J.; Tran, M.; Davenport, M.; Torres, A.; Pintus, P.; Bowers, J. Heterogeneous silicon photonics sensing for autonomous cars. *Opt. Express* **2019**, *27*, 3642. [CrossRef]
27. Ramirez, J.; Malhouitre, S.; Gradkowski, K.; Morrissey, P.; O'Brien, P.; Caillaud, C.; Vaissiere, N. III-V-on-Silicon Integration: From Hybrid Devices to Heterogeneous Photonic Integrated Circuits. *IEEE J. Sel. Top. Quantum Electron.* **2020**, *26*, 6100213. [CrossRef]
28. Van der Tol, J.; Jiao, Y.; Van Engelen, J.; Pogoretskiy, V.; Kashi, A.; Williams, K. InP Membrane on Silicon (IMOS) Photonics. *IEEE J. Quantum Electron.* **2020**, *56*, 6300107. [CrossRef]
29. Available online: https://www.diabetes.co.uk/body/white-blood-cells.html (accessed on 10 January 2023).
30. Available online: https://www.gasalarmsystems.co.uk/latest-news/3-little-known-facts-about-flammable-gas-that-could-save-your-life/ (accessed on 10 January 2023).
31. Available online: https://www.lihealthcollab.org/news-and-blog/heat-alert--heart-health-at-risk-when-temperatures-rise (accessed on 10 January 2023).
32. Huang, K.-H.; Tan, F.; Wang, T.-D.; Yang, Y.-J. A highly sensitive pressure-sensing array for blood pressure estimation assisted by machine-learning techniques. *Sensors* **2019**, *19*, 848. [CrossRef]
33. Kazanskiy, N.; Butt, M.; Khonina, S. Recent advances in wearable optical sensor automation powered by battery versus skin-like battery-free devices for personal healthcare-A review. *Nanomaterials* **2022**, *12*, 334. [CrossRef]

34. Zhang, M.; Zhang, W.; Wang, F.; Zhao, D. High-gain polymer optical waveguide amplifiers based on core-shell $NaYF_4/NaLuF_4$: Yb^{3+}, Er^{3+} NPs-PMMA covalent-linking nanocomposites. *Sci. Rep.* **2016**, *6*, 36729. [CrossRef]
35. Park, Y.-J.; Lee, S.; Kim, B.; Kim, J.-H.; So, J.-H.; Koo, H.-J. Impedance study on humidity dependent conductivity of polymer composites with conductive nanofillers. *Compos. Part B Eng.* **2020**, *202*, 108412. [CrossRef]
36. Geiss, R.; Saravi, S.; Sergeyev, A.; Diziain, S.; Setzpfandt, F.; Schrempel, F.; Grange, R.; Kley, E.-B.; Tunnermann, A.; Pertsch, T. Fabrication of nanoscale lithium niobate waveguides for second-harmonic generation. *Opt. Lett.* **2015**, *40*, 2715–2718. [CrossRef] [PubMed]
37. Eknoyan, O.; Yoon, D.; Taylor, H. Low-loss optical waveguides in lithium tantalate by vapor diffusion. *Appl. Phys. Lett.* **1987**, *51*, 384. [CrossRef]
38. Butt, M.; Kozlova, E.S.; Khonina, S.N.; Skidanov, R.V. Optical planar waveguide sensor based on (Yb,Nb): RTP/RTP(001) system for the estimation of metal coated cells. *CEUR Workshop Proc.* **2016**, *1638*, 16–23.
39. Butt, M.; Sole, R.; Pujol, M.; Rodenas, A.; Lifante, G.; Choudhary, A.; Murugan, G.; Shepherd, D.; Wilkinson, J.; Aguiló, M.; et al. Fabrication of Y-Splitters and Mach-Zehnder Structures on (Yb,Nb):$RbTiOPO_4/RbTiOPO_4$ Epitaxial Layers by Reactive Ion Etching. *J. Light. Technol.* **2015**, *33*, 1863–1871. [CrossRef]
40. Zhang, L.; Lin, Q.; Yue, Y.; Yan, Y.; Beausoleil, R.; Willner, A. Silicon waveguide with four zero-dispersion wavelengths and its application in on-chip octave-spanning supercontinuum generation. *Opt. Express* **2012**, *20*, 1685–1690. [CrossRef]
41. Senichev, A.; Peana, S.; Martin, Z.; Yesilyurt, O.; Sychev, D.; Lagutchev, A.; Boltasseva, A.; Shalaev, V. Silicon nitride waveguides with intrinsic single-photon emitters for integrated Quantum photonics. *ACS Photonics* **2022**, *9*, 3357–3365. [CrossRef]
42. Sacher, W.; Luo, X.; Yang, Y.; Chen, F.-D.; Lordello, T.; Mak, J.; Liu, X.; Hu, T.; Xue, T.; Lo, P.-Q.; et al. Visible-light silicon nitride waveguide devices and implantable neurophotonic probes on thinned 200 mm silicon wafers. *Opt. Express* **2019**, *27*, 37400–37418. [CrossRef]
43. Takenaka, M.; Nakano, Y. InP photonic wire waveguide using InAlAs oxide cladding layer. *Opt. Express* **2007**, *15*, 8422–8427. [CrossRef]
44. Soleimannezhad, F.; Nikoufard, M.; Mahdian, M. Low-loss indium phosphide-based hybrid plasmonic waveguide. *Microw. Opt. Technol. Lett.* **2021**, *63*, 2242–2251. [CrossRef]
45. Rahlves, M.; Rezem, M.; Boroz, K.; Schlangen, S.; Reithmeier, E.; Roth, B. Flexible, fast, and low-cost production process for polymer based diffractive optics. *Opt. Express* **2015**, *23*, 3614–3622. [CrossRef] [PubMed]
46. Beche, B.; Pelletier, N.; Gaviot, E.; Zyss, J. Single-mode TE00-TM00 optical waveguides on SU-8 polymer. *Opt. Commun.* **2004**, *230*, 91–94. [CrossRef]
47. Elmogi, A.; Bosman, E.; Missinne, J.; Steenberge, V. Comparison of epoxy- and siloxane-based single-mode optical waveguides defined by direct-write lithography. *Opt. Mater.* **2016**, *52*, 26–31. [CrossRef]
48. Ibrahim, M.; Kassim, N.; Mohammad, A.; Lee, S.-Y.; Chin, M.-K. Single mode optical waveguides based on photodefinable benzocyclobutene (BCB 4024-40) polymer. *Microw. Opt. Technol. Lett.* **2006**, *49*, 479–481. [CrossRef]
49. Available online: http://www.chemoptics.co.kr/eng/main/main.php (accessed on 10 January 2023).
50. Buestrich, R.; Kahlenberg, F.; Popall, M.; Dannberg, P.; Muller-Fiedler, R.; Rosch, O. ORMOCER (R) s for optical interconnection technology. *J. Sol-Gel Sci. Technol.* **2001**, *20*, 181–186. [CrossRef]
51. Bamiedakis, N.; Beals, J.; Penty, R.; White, I.; DeGroot, J.; Clapp, T. Cost-effective multimode polymer waveguides for high-speed on-board optical interconnects. *IEEE J. Quantum Electron.* **2009**, *45*, 415–424. [CrossRef]
52. Bosman, E.; Van Steenberge, G.; Christiaens, W.; Hendrickx, N.; Vanfleteren, J.; Van Daele, P. Active optical links embedded in flexible substrates. In Proceedings of the 58th Electronic Components and Technology Conference, Lake Buena Vista, FL, USA, 27–30 May 2008; pp. 1150–2013.
53. Cai, Z.; Qiu, W.; Shao, G.; Wang, W. A new fabrication method for all-PDMS waveguides. *Sens. Actuators A Phys.* **2013**, *204*, 44–47. [CrossRef]
54. Hirose, C.; Fukuda, N.; Sassa, T.; Ishibashi, K.; Ochiai, T.; Furukawa, R. Fabrication of a fluorophore-doped cylindrical waveguide structure using elastomers for visual detection of stress. *Fibers* **2019**, *7*, 37. [CrossRef]
55. Kalathimekkad, S.; Missinne, J.; Schaubroeck, D.; Mandamparambil, R. Alcohol vapor sensor based on fluorescent dye-doped optical waveguides. *IEEE Sens. J.* **2015**, *15*, 76–81. [CrossRef]
56. Marques, C.; Pospori, A.; Demirci, G.; Çetinkaya, O.; Gawdzik, B.; Antunes, P.; Bang, O.; Mergo, P.; André, P.; Webb, D. Fast Bragg Grating Inscription in PMMA Polymer Optical Fibres: Impact of Thermal Pre-Treatment of Preforms. *Sensors* **2017**, *17*, 891. [CrossRef]
57. Woyessa, G.; Theodosiou, A.; Markos, C.; Kalli, K.; Bang, O. Single Peak Fiber Bragg Grating Sensors in Tapered Multimode Polymer Optical Fibers. *J. Light. Technol.* **2021**, *39*, 6934–6941. [CrossRef]
58. Pasquardini, L.; Cennamo, N.; Malleo, G.; Vanzetti, L.; Zeni, L.; Bonamini, D.; Salvia, R.; Bassi, C.; Bossi, A. A Surface Plasmon Resonance Plastic Optical Fiber Biosensor for the Detection of Pancreatic Amylase in Surgically-Placed Drain Effluent. *Sensors* **2021**, *21*, 3443. [CrossRef] [PubMed]
59. Kadhim, R.A.; Abdul, K.K.; Yuan, L. Advances in Surface Plasmon Resonance-Based Plastic Optical Fiber Sensors. *IETE Tech. Rev.* **2022**, *39*, 442–459. [CrossRef]
60. Cennamo, N.; Pesavento, M.; Zeni, L. A review on simple and highly sensitive plastic optical fiber probes for bio-chemical sensing. *Sens. Actuators B Chem.* **2021**, *331*, 129393. [CrossRef]

61. Rajamani, A.S.; Divagar, M.; Sai, V. Plastic fiber optic sensor for continuous liquid level monitoring. *Sens. Actuators A Phys.* **2019**, *296*, 192–199. [CrossRef]
62. Prajzler, V.; Neruda, M.; Jasek, P.; Nekvindova, P. The properties of free-standing epoxy polymer multi-mode optical waveguides. *Microsyst. Technol.* **2019**, *25*, 257–264. [CrossRef]
63. Kagami, M.; Kawasaki, A.; Ito, H. A polymer optical waveguide with out-of-plane branching mirrors for surface-normal optical interconnections. *J. Light. Technol.* **2001**, *19*, 1949–1955. [CrossRef]
64. Klein, S.; Barsella, A.; Leblond, H.; Bulou, H.; Fort, A.; Andraud, C.; Lemercier, G.; Mulatier, J.; Dorkenoo, K. One-step waveguide and optical circuit writing in photopolymerizable materials processed by two-photon absorption. *Appl. Phys. Lett.* **2005**, *86*, 211118. [CrossRef]
65. Wong, W.; Zhou, J.; Pun, E. Low-loss polymeric optical waveguides using electron-beam direct writing. *Appl. Phys. Lett.* **2001**, *78*, 2110–2112. [CrossRef]
66. Choi, C.-G.; Kim, J.-T.; Jeong, M.-Y. Fabrication of optical waveguides in thermosetting polymers using hot embossing. In Proceedings of the Integrated Photonics Research, Washington, DC, USA, 15–20 June 2003.
67. Choi, C.-G.; Han, S.-P.; Kim, B.-C.; Ahn, S.-H.; Jeong, M.-Y. Fabrication of large-core 1 × 16 optical power splitters in polymers using hot-embossing process. *IEEE Photon. Technol. Lett.* **2003**, *15*, 825–827. [CrossRef]
68. Zheng, L.; Keppler, N.; Zhang, H.; Behrens, P.; Roth, B. Planar polymer optical waveguide with metal-organic framework coating for carbon dioxide sensing. *Adv. Mater. Technol.* **2022**, *7*, 2200395. [CrossRef]
69. Fan, R.; Hooker, R. Tapered polymer single-mode waveguides for mode transformation. *J. Light. Technol.* **1999**, *17*, 466–474. [CrossRef]
70. Kobayashi, J.; Yagi, S.; Hatakeyama, Y.; Kawakami, N. Low loss polymer optical waveguide replicated from flexible film stamp made of polymeric material. *Jpn. J. Appl. Phys.* **2013**, *52*, 072501. [CrossRef]
71. Bruck, R.; Muellner, P.; Kataeva, N.; Koeck, A.; Trassl, S.; Rinnerbauer, V.; Schmidegg, K.; Hainberger, R. Flexible thin-film polymer waveguides fabricated in an industrial roll-to-roll process. *Appl. Opt.* **2013**, *52*, 4510–4514. [CrossRef]
72. Shneidman, A.; Becker, K.; Lukas, M.; Torgerson, N.; Wang, C.; Reshef, O.; Burek, M.; Paul, K.; McLellan, J.; Loncar, M. All-polymer integrated optical resonators by roll-to-roll nanoimprint lithography. *ACS Photonics* **2018**, *5*, 1839–1845. [CrossRef]
73. Shao, J.; Chen, X.L.; Li, X.; Tian, H.; Wang, C.; Lu, B. Nanoimprint lithography for the manufacturing of flexible electronics. *Sci. China Technol. Sci.* **2019**, *62*, 175–198. [CrossRef]
74. Šakalys, R.; Kho, K.; Keyes, T. A reproducible, low cost microfluidic microcavity array SERS platform prepared by soft lithography from a 2 photon 3D printed template. *Sens. Actuators B Chem.* **2021**, *340*, 129970. [CrossRef]
75. Azadegan, R.; Nagarajan, P.; Yao, D.; Ellis, T. Polymer micro hot embossing for the fabrication of three-dimensional millimeter-wave components. In Proceedings of the IEEE Antennas and Propagation Society International Symposium, Charleston, SC, USA, 1–5 June 2009; pp. 1–4.
76. Aldada, L.; Shacklette, L. Advances in polymer integrated optics. *IEEE J. Sel. Top. Quant.* **2000**, *6*, 54–68. [CrossRef]
77. Andolfi, L.; Greco, S.L.M.; Tierno, D.; Chignola, R.; Martinelli, M.; Giolo, E.; Luppi, S.; Delfino, I.; Zanetti, M.; Battistella, A.; et al. Planar AFM macro-probes to study the biomechanical properties of large cells and 3D cell spheroids. *Acta Biomater.* **2019**, *94*, 505–513. [CrossRef]
78. Norland Optical Adhesive 73. Available online: https://www.amstechnologies-webshop.com/media/pdf/09/bb/1a/NOA-73-TDS-Datasheet.pdf (accessed on 13 February 2023).
79. Santiago-Alvarado, A.; Cruz-Felix, A.; Iturbide, F.; Licona-Morán, B. Physical-chemical properties of PDMS samples used in tunable lenses. *Int. J. Eng. Sci. Innov. Technol.* **2014**, *3*, 563–571.
80. Johnston, D.; McCluskey, D.K.; Tan, C.K.L.; Tracey, M.C. Mechanical characterization of bulk Sylgard 184 for microfluidics and microengineering. *J. Micromech. Microeng.* **2014**, *24*, 035017. [CrossRef]
81. Cai, D.K.; Neyer, A.; Kuckuk, R.; Heise, H.M. Optical absorption in transparent PDMS materials applied for multimode waveguides fabrication. *Opt. Mater.* **2008**, *30*, 1157–1161. [CrossRef]
82. Khan, Y.; Butt, M.; Khonina, S.; Kazanskiy, N. Thermal sensor based on polydimethylsiloxane polymer deposited on low-index-contrast dielectric photonic crystal structure. *Photonics* **2022**, *9*, 770. [CrossRef]
83. Demir, M.M.; Koynov, K.; Akbey, Ü.; Bubeck, C.; Park, I.; Lieberwirth, I.; Wegner, G. Optical Properties of Composites of PMMA and Surface-Modified Zincite Nanoparticles. *Macromolecules* **2007**, *40*, 1089–1100. [CrossRef]
84. Abdelrazek, E.M.; Hezma, A.M.; El-khodary, A.; Elzayat, A.M. Spectroscopic studies and thermal properties of PCL/PMMA biopolymer blend. *Egypt. J. Basic Appl. Sci.* **2016**, *3*, 10–15. [CrossRef]
85. Ishiyama, C.; Higo, Y. Effects of humidity on Young's modulus in poly(methyl methacrylate). *J. Polym. Sci. Part B Polym. Phys.* **2002**, *40*, 460–465. [CrossRef]
86. Min, R.; Hu, X.; Pereira, L.; Soares, M.S.; Silva, L.C.B.; Wang, G.; Martins, L.; Qu, H.; Antunes, P.; Marques, C.; et al. Polymer optical fiber for monitoring human physiological and body function: A comprehensive review on mechanisms, materials, and applications. *Opt. Laser Technol.* **2022**, *147*, 107626. [CrossRef]
87. Beadie, G.; Brindza, M.; Flynn, R.A.; Rosenberg, A.; Shirk, J.S. Refractive index measurements of poly(methyl methacrylate) (PMMA) from 0.4–1.6 µm. *Appl. Opt.* **2015**, *54*, F139–F143. [CrossRef]
88. NOA68. Available online: https://www.norlandprod.com/adhesives/noa%2068.html (accessed on 13 February 2023).

89. Sabzekar, M.; Chenar, M.P.; Maghsoud, Z.; Mostaghisi, O.; García-Payo, M.C.; Khayet, M. Cyclic olefin polymer as a novel membrane material for membrane distillation applications. *J. Membr. Sci.* **2021**, *621*, 118845. [CrossRef]
90. Khanarian, G. Optical properties of cyclic olefin copolymers. *Opt. Eng.* **2001**, *40*, 1024–1029. [CrossRef]
91. Schmid, S. *Electrostatically Actuated All-Polymer Microbeam Resonators—Characterization and Application*; ETH Zurich: Zurich, Switzerland, 2009.
92. Lee, B.; Choi, K.-H.; Yoo, K. Innovative SU-8 Lithography Techniques and Their Applications. *Micromachines* **2015**, *6*, 1–18. [CrossRef]
93. Wolter, H.; Storch, W.; Ott, H. New Inorganic/Organic Copolymers (Ormocer®s) for Dental Applications. *MRS Online Proc. Libr.* **1994**, *346*, 143. [CrossRef]
94. Schmidt, V.; Kuna, L.; Satzinger, V.; Houbertz, R.; Jakopic, G.; Leising, G. Application of two-photon 3D lithography for the fabrication of embedded ORMOCER waveguides. In Proceedings of the Optoelectronic Integrated Circuits IX, San Jose, CA, USA, 22–24 January 2007.
95. Declerck, P.; Houbertz, R.; Jakopic, G.; Passinger, S.; Chichkov, B. High Refractive Index Inorganic-Organic Hybrid Materials for Photonic Applications. *MRS Online Proc. Libr.* **2007**, *1007*, 1007. [CrossRef]
96. Mahdi, E.M.; Chaudhuri, A.K.; Tan, J.-C. Capture and immobilisation of iodine (I 2) utilising polymer-based ZIF-8 nanocomposite membranes. *Mol. Syst. Des. Eng.* **2016**, *1*, 122–131. [CrossRef]
97. Keppler, N.C.; Hindricks, K.D.J.; Behrens, P. Large refractive index changes in ZIF-8 thin films of optical quality. *RSC Adv.* **2022**, *12*, 5807–5815. [CrossRef]
98. Kazanskiy, N.L.; Butt, M.A.; Khonina, S.N. Carbon Dioxide Gas Sensor Based on Polyhexamethylene Biguanide Polymer Deposited on Silicon Nano-Cylinders Metasurface. *Sensors* **2021**, *21*, 378. [CrossRef]
99. Wang, J.; Luo, Y.; Jin, K.; Yuan, C.; Sun, J.; He, F.; Fang, Q. A novel one-pot synthesized organosiloxane: Synthesis and conversion to directly thermo-crosslinked polysiloxanes with low dielectric constants and excellent thermostability. *Polym. Chem.* **2015**, *6*, 5984–5988. [CrossRef]
100. Kane, C.F.; Krchnavek, R.R. Benzocyclobutene optical waveguides. *IEEE Photonics Technol. Lett.* **1995**, *7*, 535–537. [CrossRef]
101. Guo, S.; Gustafsson, G.; Hagel, O.J.; Arwin, H. Determination of refractive index and thickness of thick transparent films by variable-angle spectroscopic ellipsometry: Application to benzocyclobutene films. *Appl. Opt.* **1996**, *35*, 1693–1699. [CrossRef]
102. Wang, J.; Chen, C.; Wang, C.; Wang, X.-B.; Yi, Y.; Sun, X.; Wang, F.; Zhang, D. Metal-Printing Defined Thermo-Optic Tunable Sampled Apodized Waveguide Grating Wavelength Filter Based on Low Loss Fluorinated Polymer Material. *Appl. Sci.* **2019**, *10*, 167. [CrossRef]
103. NOA63. Available online: https://www.norlandprod.com/adhesives/noa%2063.html (accessed on 13 February 2023).
104. Bucknall, C.B.; Gilbert, A.H. Toughening tetrafunctional epoxy resins using polyetherimide. *Polymer* **1989**, *30*, 213–217. [CrossRef]
105. Wang, X.; Wang, Y.; Bi, S.; Wang, Y.; Chen, X.; Qiu, L.; Sun, J. Optically Transparent Antibacterial Films Capable of Healing Multiple Scratches. *Adv. Funct. Mater.* **2014**, *24*, 403–411. [CrossRef]
106. Jiang, F.; Cakmak, M. Real time optical and mechano-optical studies during drying and uniaxial stretching of Polyetherimide films from solution. *Polymer* **2015**, *68*, 168–175. [CrossRef]
107. Vinogradova, I.; Andrienko, D.; Lulevich, V.V.; Nordschild, S.; Sukhorukov, G.B. Young's Modulus of Polyelectrolyte Multilayers from Microcapsule Swelling. *Macromolecules* **2004**, *37*, 1113–1117. [CrossRef]
108. Kim, J.-H.; Fujita, S.; Shiratori, S. Design of a thin film for optical applications, consisting of high and low refractive index multilayers, fabricated by a layer-by-layer self-assembly method. *Colloids Surf. A Physicochem. Eng. Asp.* **2006**, *284–285*, 290–294. [CrossRef]
109. Liang, Y.; Zhao, M.; Wu, Z.; Morthier, G. Investigation of Grating-Assisted Trimodal Interferometer Biosensors Based on a Polymer Platform. *Sensors* **2018**, *18*, 1502. [CrossRef] [PubMed]
110. Bosc, D.; Maalouf, A.; Messaad, K.; Mahé, H.; Bodiou, L. Advanced analysis of optical loss factors in polymers for integrated optics circuits. *Opt. Mater.* **2013**, *35*, 1207–1212. [CrossRef]
111. Kaino, T. Plastic optical fibers. In *Polymers in Optics: Physics, Chemistry, and Applications: A Critical Review*; Society of Photo Optical Loaction: Bellingham, WA, USA, 1996.
112. Butt, A.M.; Kazanskiy, N.L.; Khonina, S.N. Highly integrated plasmonic sensor design for the simultaneous detection of multiple analytes. *Curr. Appl. Phys.* **2020**, *20*, 1274–1280. [CrossRef]
113. Butt, A.M.; Voronkov, G.; Grakhova, E.; Kutluyarov, R.; Kazanskiy, N.; Khonina, S. Environmental Monitoring: A Comprehensive Review on optical waveguide and fiber-based sensors. *Biosensors* **2022**, *12*, 1038. [CrossRef]
114. Butt, A.M. Numerical investigation of a small footprint plasmonic Bragg grating structure with a high extinction ratio. *Photonics Lett. Pol.* **2020**, *12*, 82–84. [CrossRef]
115. Butt, M.A.; Khonina, S.N.; Kazanskiy, N.L. A plasmonic colour filter and refractive index sensor applications based on metal-insulator-metal square micro-ring cavities. *Laser Phys.* **2020**, *30*, 016205. [CrossRef]
116. Butt, M.A.; Khonina, S.N.; Kazanskiy, N.L. Hybrid plasmonic waveguide-assisted metal-insulator-metal ring resonator for refractive index sensing. *J. Mod. Opt.* **2018**, *65*, 1135–1140. [CrossRef]
117. Butt, M.A.; Khonina, S.N.; Kazanskiy, N.L. Sensitivity enhancement of silicon strip waveguide ring resonator by incorporating a thin metal film. *IEEE Sens. J.* **2020**, *3*, 1355–1362. [CrossRef]

118. Butt, M.A.; Degtyarev, S.A.; Khonina, S.N.; Kazanskiy, N.L. An evanescent field absorption gas sensor at mid-IR 3.39 um wavelength. *J. Mod. Opt.* **2017**, *64*, 1892–1897. [CrossRef]
119. Sonawane, H.; Singh, A.; Gupta, A.; Tiwari, M.; Gaur, S. Polymer based surface plasmon resonance sensors: Theoretical study of sensing characteristics. *Mater. Proc.* **2022**, *67*, 726–731. [CrossRef]
120. Sahraeibelverdi, T.; Guo, L.; Veladi, H.; Malekshahi, M. Polymer ring resonator with a partially tapered waveguide for biomedical sensing: Computational study. *Sensors* **2021**, *21*, 5017. [CrossRef]
121. Moraresecu, R.; Pal, P.; Beneitez, N.; Missinne, J.; Steenberge, G.; Bienstman, P.; Morthier, G. Fabrication and characterization of high-optical-quality factor hybrid polymer microring resonators operating at very near infrared wavelengths. *IEEE Photonics J.* **2016**, *8*, 6600409. [CrossRef]
122. Ma, X.; Zhao, Z.; Yao, H.; Deng, J.; Wu, J.; Hu, Z.; Chen, K. Compact and highly sensitive refractive index sensor based on embedded double-ring resonator using Vernier effect. *IEEE Photonics J.* **2022**, *15*, 6800109. [CrossRef]
123. Xiao, Y.; Hofmann, M.; Wang, Z.; Sherman, S.; Zappe, H. Design of all-polymer asymmetric Mach-Zehnder interferometer sensors. *Appl. Opt.* **2016**, *55*, 3566–3573. [CrossRef]
124. Ji, L.; Yang, S.; Shi, R.; Fu, Y.; Su, J.; Wu, C. Polymer waveguide coupled surface plasmon refractive index sensor: A theoretical study. *Photonic Sens.* **2020**, *10*, 353–363. [CrossRef]
125. Mancuso, M.; Goddard, J.; Erickson, D. Nanoporous polymer ring resonators for biosensing. *Opt. Express* **2011**, *20*, 245–255. [CrossRef]
126. Dullo, F.; Lindecrantz, S.; Jagerska, J.; Hansen, J.; Engqvist, M.; Solbo, S.; Helleso, O. Sensitive on-chip methane detection with a cryptophane- A cladded Mach-Zehnder interferometer. *Opt. Express* **2015**, *23*, 31564–31573. [CrossRef] [PubMed]
127. Lin, B.; Yi, Y.; Cao, Y.; Lv, J.; Yang, Y.; Wang, F.; Sun, X.; Zhang, D. A polymer asymmetric Mach-Zehnder interferometer sensor model based on electrode thermal writing waveguide technology. *Micromachines* **2019**, *10*, 628. [CrossRef] [PubMed]
128. Chen, S.; Lin, C. Sensitivity comparison of graphene based surface plasmon resonance biosensor with Au, Ag and Cu in the visible region. *Mater. Res. Express* **2019**, *6*, 056503. [CrossRef]
129. Ceylan, K.H.; Kulah, H.; Ozgen, C. Thin film biosensors. In *Thin Films and Coatings in Biology. Biological and Medical Physics, Biomedical Engineering*; Springer: Dordrecht, The Netherlands, 2013.
130. Bahabady, A.; Olyaee, S. Two-curve-shaped biosensor for detecting glucose concentration and salinity of seawater based on photonic crystal nano-ring resonator. *Sens. Lett.* **2015**, *13*, 774–777. [CrossRef]
131. Xu, D.-X.; Vachon, M.; Densmore, A.; Ma, R.; Janz, S.; Delâge, A.; Lapointe, J.; Cheben, P.; Schmid, J.H.; Post, E.; et al. Real-time cancellation of temperature induced resonance shifts in SOI wire waveguide ring resonator label-free biosensor arrays. *Opt. Express* **2010**, *18*, 22867–22879. [CrossRef]
132. Guo, J.; Yang, C.; Dai, Q.; Kong, L. Wearable and biomedical applications. *Sensors* **2019**, *19*, 3771. [CrossRef]
133. Ahmed, Z.; Reddy, J.; Malekoshoaraie, M.; Hassanzade, V.; Kimukin, I.; Jain, V.; Chamanzar, M. Flexible optoelectric neural interfaces. *Curr. Opin. Biotechnol.* **2021**, *72*, 121–130. [CrossRef]
134. Ang, L.; Por, L.; Yam, M. Study on different molecular weights of chitosan as an immobilization matrix for a glucose biosensor. *PLoS ONE* **2013**, *8*, e70597. [CrossRef]
135. Bucur, B.; Purcarea, C.; Andreescu, S.; Vasilescu, A. Addressing the selectivity of enzyme biosensors: Solutions and percpectives. *Sensors* **2021**, *21*, 3038. [CrossRef]
136. Lavin, A.; Vicente, J.; Holgado, M.; Laguna, M.; Casquel, R.; Santamaria, B.; Maigler, M.; Hernandez, A.; Ramirez, Y. On the determination of uncertainty and limit of detection in label-free biosensors. *Sensors* **2018**, *18*, 2038. [CrossRef] [PubMed]
137. Chen, L.-C.; Wang, E.; Tai, C.-S.; Chiu, Y.-C.; Li, C.-W.; Lin, Y.-R.; Lee, T.-H.; Huang, C.-W.; Chen, J.-C.; Chen, W. Improving the reproducibility, accuracy, and stability of an electrochemical biosensor platform for point-of-care use. *Biosens. Bioelectron.* **2020**, *155*, 112111. [CrossRef] [PubMed]
138. Bruck, R.; Hainberger, R. Polymer waveguide based biosensor. In *Photonics, Devices, and Systems IV*; SPIE: Bellingham, WA, USA, 2008.
139. Wang, C.; Yi, P.; Li, J.; Dong, H.; Chen, C.; Zhang, D.; Shen, H.; Fu, B. Polymer optical waveguide grating-based biosensor to detect effective drug concentrations of Ginkgolide A for Inhibition of PMVEC apoptosis. *Biosensors* **2021**, *11*, 264. [CrossRef] [PubMed]
140. Wang, M.; Hiltunen, J.; Liedert, C.; Pearce, S.; Charlton, M.; Hakalahti, L.; Karioja, P.; Myllyla, R. Highly sensitive biosensor based on UV-imprinted layered polymeric-inorganic composite waveguides. *Opt. Express* **2012**, *20*, 20309–20317. [CrossRef]
141. Walter, J.-G.; Eilers, A.; Alwis, L.; Roth, B.; Bremer, K. SPR Biosensor Based on Polymer Multi-Mode Optical Waveguide and Nanoparticle Signal Enhancement. *Sensors* **2020**, *20*, 2889. [CrossRef]
142. Han, X.-Y.; Wu, Z.-L.; Yang, S.-C.; Shen, F.-F.; Liang, Y.-X.; Wang, L.-H.; Wang, J.-Y.; Ren, J.; Jia, L.-Y.; Zhang, H.; et al. Recent progress of imprinted polymer photonic waveguide devices and applications. *Polymers* **2018**, *10*, 603. [CrossRef]
143. Nguyen, H.D.; Hollenbach, U.; Pfirrmann, S.; Ostrizinski, U.; Pfeiffer, K.; Hengsbach, S.; Mohr, J. Photo-structurable polymer for interlayer single-mode waveguide fabrication by femtosecond laser writing. *Opt. Mater.* **2017**, *66*, 110–116. [CrossRef]
144. Yi, L.; Changyuan, Y. Highly strechable hybrid silica/polymer optical fiber sensors for large-strain and high-temperature application. *Opt. Express* **2019**, *27*, 20107–20116. [CrossRef]
145. Wang, T.; Hu, S.; Chamlagain, B.; Hong, T.; Zhou, Z.; Weiss, S.; Xu, Y.-Q. Visualizing light scattering in silicon waveguides with black phosphorus photodetectors. *Adv. Mater.* **2016**, *28*, 7162–7166. [CrossRef]

146. Mirnaziry, S.; Wolff, C.; Steel, M.; Eggleton, B.; Poulton, C. Stimulated Brillouin scattering in silicon/chalcogenide slot waveguides. *Opt. Express* **2016**, *24*, 4786–4800. [CrossRef]
147. Kumaar, S.; Sivasubramanian, A. Analysis of BCB and SU 8 photonic waveguide in MZI architecture for point-of-care devices. *Sens. Int.* **2023**, *4*, 100207. [CrossRef]
148. Ramirez, J.; Lechuga, L.; Gabrielli, L.; Hernandez-Figueroa, H. Study of a low-cost trimodal polymer waveguide for interferometric optical biosensors. *Opt. Express* **2015**, *23*, 11985. [CrossRef] [PubMed]
149. Walter, J.-G.; Alwis, L.; Roth, B.; Bremer, K. All-Optical Planar Polymer Waveguide-Based Biosensor Chip Designed for Smartphone-Assisted Detection of Vitamin D. *Sensors* **2020**, *20*, 6771. [CrossRef] [PubMed]
150. Tu, X.; Chen, S.-L.; Song, C.; Huang, T.; Guo, L. Ultrahigh Q polymer microring resonators for biosensing applications. *IEEE Photonics J.* **2019**, *11*, 4200110. [CrossRef]
151. Girschikofsky, M.; Rosenberger, M.; Belle, S.; Brutschy, M.; Waldvogel, S.; Hellmann, R. Optical planar Bragg grating sensor for real-time detection of benzene, toluene and xylene in solvent vapour. *Sens. Actuators B Chem.* **2012**, *171–172*, 338–342. [CrossRef]
152. Zaky, Z.; Ahmed, A.; Shalaby, A.; Aly, A. Refractive index gas sensor based on the Tamm state in a one-dimensional photonic crystal: Theoretical optimisation. *Sci. Rep.* **2020**, *10*, 9736. [CrossRef]
153. Butt, M.A.; Khonina, S.N.; Kazanskiy, N.L. Modelling of rib channel waveguides based on silicon-on-sapphire at 4.67 um wavelength for evanescent field gas absorption sensor. *Optik* **2018**, *168*, 692–697. [CrossRef]
154. Kazanskiy, N.; Khonina, S.; Butt, M. Polarization-insensitive hybrid plasmonic waveguide design for evanescent field absorption gas sensor. *Photonic Sens.* **2021**, *11*, 279–290. [CrossRef]
155. Wanguemert-Perez, J.; Cheben, P.; Ortega-Monux, A.; Alonso-Ramos, C.; Perez-Galacho, D.; Halir, R.; Molina-Fernandez, I.; Xu, D.-X.; Schmid, J. Evanescent field waveguide sensing with subwavelength grating structures in silicon-on-insulator. *Opt. Lett.* **2014**, *39*, 4442–4445. [CrossRef]
156. Nylabder, C.; Armgrath, M.; Lundstrom, I. An ammonia detector based on a conducting polymer. In Proceedings of the International Meeting on Chemical Sensors, Fukuoka, Japan, 19–22 September 1983; pp. 203–207.
157. Hopper, R.; Popa, D.; Udrea, F.; Ali, S.; Stanley-Marbell, P. Miniaturized thermal acoustic gas sensor based on a CMOS microhotplate and MEMS microphone. *Sci. Rep.* **2022**, *12*, 1690. [CrossRef]
158. Sadaoka, Y.; Sakai, Y.; Manabe, T. Detection of CO_2 using a solid-state electrochemical sensor based on sodium ionic conductors. *Sens. Actuators B Chem.* **1993**, *15*, 166–170. [CrossRef]
159. Lin, Z.-D.; Young, S.-J.; Chang, S.-J. CO_2 gas sensors based on carbon nanotube thin films using a simple transfer method on flexible substrate. *IEEE Sens. J.* **2015**, *15*, 7017–7020. [CrossRef]
160. Gheorghe, A.; Lugier, O.; Ye, B.; Tanase, S. Metal-organic framework based systems for CO_2 sensing. *J. Mater. Chem. C* **2021**, *9*, 16132–16142. [CrossRef]
161. Nugroho, F.; Darmadi, I.; Cusinato, L.; Susarrey-Arce, A.; Schreuders, H.; Bannenberg, L.; Fanta, A.; Kadkhodazadeh, S.; Wagner, J.; Antosiewicz, T.; et al. Metal-polymer hybrid nanomaterials for plasmonic ultrafast hydrogen detection. *Nat. Mater.* **2019**, *18*, 489–495. [CrossRef] [PubMed]
162. Bamiedakis, N.; Hutter, T.; Penty, R.; Elliott, S. PCB-integrated optical waveguide sensors: An ammonia gas sensor. *J. Light. Technol.* **2013**, *31*, 1628. [CrossRef]
163. Batumalay, M.; Johari, A.; Khudus, M.I.M.A.; Bin Jali, M.H.; Al Noman, A.; Harun, S.W. Microbottle resonator for temperature sensing. *J. Phys. Conf. Ser.* **2019**, *1371*, 012006. [CrossRef]
164. Kong, Y.; Wei, Q.; Liu, C.; Wang, S. Nanoscale temperature sensor based on Fano resonance in metal-insulator-metal waveguide. *Opt. Commun.* **2017**, *384*, 85–88. [CrossRef]
165. Butt, M.; Khonina, S.; Kazanskiy, N. A compact design of a modified Bragg grating filter based on a metal-insulator-metal waveguide for filtering and temperature sensing applications. *Optik* **2022**, *251*, 168466. [CrossRef]
166. Butt, M.; Kazanskiy, N.; Khonina, S. Revolution in flexible wearable electronics for temperature and pressure monitoring—A review. *Electronics* **2022**, *11*, 716. [CrossRef]
167. Roth, G.-L.; Hessler, S.; Kefer, S.; Girchikofsky, M.; Esen, C.; Hellmann, R. Femtosecond laser inscription of waveguides and Bragg gratings in transparent cyclic olefin copolymers. *Opt. Express* **2020**, *28*, 18077–18084. [CrossRef]
168. Missinne, J.; Beneitez, N.; Lamberti, A.; Chiesura, G.; Luyckx, G.; Mattelin, M.-A.; Paepegem, W.; Steenberge, G. Thin and flexible polymer photonic sensor foils for moniitoring composite structures. *Adv. Eng. Mater.* **2018**, *20*, 1701127. [CrossRef]
169. Butt, M.; Kazanskiy, N.; Khonina, S. Advances in Waveguide Bragg Grating Structures, Platforms, and Applications: An Up-to-Date Appraisal. *Biosensors* **2022**, *12*, 497. [CrossRef]
170. Eldada, L.; Blomquist, R.; Maxfield, M.; Pant, D.; Boudoughian, G.; Poga, C.; Norwood, R. Thermooptic planar polymer Bragg grating OADMs with broad tuning range. *IEEE Photon. Technol. Lett.* **1999**, *11*, 448–450. [CrossRef]
171. Yun, B.; Hu, G.; Cui, Y. Third-order polymer waveguide Bragg grating array by using conventional contact lithography. *Opt. Commun.* **2014**, *330*, 113–116. [CrossRef]
172. Binfeng, Y.; Guohua, H.; Yiping, C. Polymer waveguide Bragg grating Fabry-Perot filter using a nanoimprinting technique. *J. Opt.* **2014**, *16*, 105501. [CrossRef]
173. Song, F.; Xiao, J.; Xie, A.; Seo, S.-W. A polymer waveguide grating sensor integrated with a thin-film photodetector. *J. Opt.* **2014**, *16*, 015503. [CrossRef]

174. Lin, H.; Xing, Y.; Chen, X.; Zhang, S.; Forsberg, E.; He, S. Polymer-based planar waveguide chirped Bragg grating for high-resolution tactile sensing. *Opt. Express* **2022**, *30*, 20871–20882. [CrossRef]
175. Rosenberger, M.; Eisenbeil, W.; Schmauss, B.; Hellmann, R. Simultaneous 2D strain sensing using polymer planar Bragg gratings. *Sensors* **2015**, *15*, 4264–4272. [CrossRef]
176. Wang, M.; Hiltunen, J.; Uusitalo, S.; Puustinen, J.; Lappalainen, J.; Karioja, P.; Myllylä, R. Fabrication of optical inverted-rib waveguides using UV-imprinting. *Microelectron. Eng.* **2011**, *88*, 175–178. [CrossRef]
177. Beneitez, N.; Missinne, J.; Shi, Y.; Chiesura, G.; Luyckx, G.; Degrieck, J.; Steenberge, G. Highly sensitive waveguide Bragg grating temperature sensor using hybrid polymers. *IEEE Photonics Technol. Lett.* **2016**, *28*, 1150. [CrossRef]
178. Khan, M.; Farooq, H.; Wittmund, C.; Klimke, S.; Lachmayer, R.; Renz, F.; Roth, B. Polymer optical waveguide sensor based on Fe-Amino-Triazole complex molecular switches. *Polymers* **2021**, *13*, 195. [CrossRef]
179. Liu, Y.; Li, M.; Zhao, P.; Wang, X.; Qu, S. High sensitive temperature sensor based on a polymer waveguide integrated in an optical fibre micro-cavity. *J. Opt.* **2018**, *20*, 015801. [CrossRef]
180. Niu, D.; Wang, L.; Xu, Q.; Jiang, M.; Wang, X.; Sun, X.; Wang, F.; Zhang, D. Ultra-sensitive polymeric waveguide temperature sensor based on asymmetric Mach-Zehnder interferometer. *Appl. Opt.* **2019**, *58*, 1276–1280. [CrossRef]
181. Wang, C.; Zhang, D.; Yue, J.; Zhang, X.; Wu, Z.; Zhang, T.; Chen, C.; Fei, T. Optical waveguide sensors for measuring human temperature and humidity with gel polymer electrolytes. *ACS Appl. Mater. Interfaces* **2021**, *13*, 60384–60392. [CrossRef]
182. Nazempour, R.; Zhang, Q.; Fu, R.; Sheng, X. Biocompatible and implantable optical fibers and waveguides for biomedicine. *Materials* **2018**, *11*, 1283. [CrossRef]
183. Hah, D.; Yoon, E.; Hong, S. An optomechanical pressure sensor using multimode interference couplers with polymer waveguides on a thin p+-Si membrane. *Sens. Actuators* **2000**, *79*, 204–210. [CrossRef]
184. Ren, Y.; Mormile, P.; Petti, L.; Cross, G. Optical waveguide humidity sensor with symmetric multilayer configuration. *Sens. Actuators B Chem.* **2001**, *75*, 76–82. [CrossRef]
185. Guo, J.; Zhou, B.; Yang, C.; Dai, Q.; Kong, L. Stretchable and temperature-sensitive polymer optical fibers for wearable health monitoring. *Adv. Funct. Mater.* **2019**, *29*, 1902898. [CrossRef]
186. Yun, S.; Park, S.; Park, B.; Kim, Y.; Park, S.; Nam, S.; Kyung, K. Polymer-waveguide-based flexible tactile sensor array for dynamic response. *Adv. Mater.* **2014**, *26*, 4474–4480. [CrossRef]
187. Song, Y.; Peters, K. A self-repairing polymer waveguide sensor. *Smart Mater. Struct.* **2011**, *20*, 065005. [CrossRef]
188. Guo, J.; Liu, X.; Jiang, N.; Yetisen, A.; Yuk, H.; Yang, C.; Khademhosseini, A.; Zhao, X.; Yun, S. Highly stretchable, strain sensing hydrogel optical fibers. *Adv. Mater.* **2016**, *28*, 10244–10249. [CrossRef]
189. Niu, D.; Wang, X.; Sun, S.; Jiang, M.; Xu, Q.; Wang, F.; Wu, Y.; Zhang, D. Polymer/silica hybrid waveguide temperature sensor based on asymmetric Mach-Zehnder interferometer. *J. Opt.* **2018**, *20*, 045803. [CrossRef]
190. Mares, D.; Prajzler, V.; Martan, T.; Jerabek, V. Hybrid polymer–glass planar Bragg grating as a temperature and humidity sensor. *Opt. Quantum Electron.* **2022**, *54*, 590. [CrossRef]
191. Kefer, S.; Rosenberger, M.; Hessler, S.; Girschikofsky, M.; Belle, S.; Roth, G.-L.; Schmauss, B. Fabrication and applications of polymer planar Bragg grating sensors based on cyclic olefin copolymers. In Proceedings of the Photonics & Electromagnetics Research Symposium-Fall (PIERS-Fall), Xiamen, China, 17–20 December 2019; pp. 647–655.
192. Butt, M.; Khonina, S.; Kazanskiy, N.; Piramidowicz, R. Hybrid metasurface perfect absorbers for temperature and biosensing applications. *Opt. Mater.* **2022**, *123*, 111906. [CrossRef]
193. Li, J.; Zhao, C.; Dong, Q.; Kang, J.; Shen, C.; Wang, D. Multipoint temperature sensor based on PDMS-filled Fabry Perot interferometer with an array-waveguide grating. In Proceedings of the 18th International Conference on Optical Communications and Networks (ICOCN), Huangshan, China, 5–8 August 2019; pp. 1–3.
194. Ramirez, J.; Gabrielli, L.; Lechuga, L.; Hernandez-Figueroa, H. Trimodal Waveguide Demonstration and Its Implementation as a High Order Mode Interferometer for Sensing Application. *Sensors* **2019**, *19*, 2821. [CrossRef]
195. Missinne, J.; Beneitez, N.; Mattelin, M.-A.; Lamberti, A.; Luyckx, G.; Paepegem, W.; Steenberge, G. Bragg-Grating-Based Photonic Strain and Temperature Sensor Foils Realized Using Imprinting and Operating at Very Near Infrared Wavelengths. *Sensors* **2018**, *18*, 2717. [CrossRef]
196. Butt, M.; Kazanskiy, N.; Khonina, S. On-chip symmetrically and asymmetrically transformed plasmonic Bragg grating formation loaded with a functional polymer for filtering and CO_2 gas sensing applications. *Measurement* **2022**, *201*, 111694. [CrossRef]
197. Lim, J.; Kim, S.; Kim, J.-S.; Kim, J.; Kim, Y.; Lim, J.; Im, Y.; Park, J.; Hann, S. Polymer waveguide sensor with tin oxide thin film integrated onto optical-electrical printed circuit board. In *Optical Micro-and Nanometrology V*; SPIE: Brussels, Belgium, 2014; Volume 9132.
198. Clevenson, H.; Desjardins, P.; Gan, X.; Englund, D. High sensitivity gas sensor based on high-Q suspended polymer photonic crystal nanocavity. *Appl. Phys. Lett.* **2014**, *104*, 241108. [CrossRef]
199. Khonina, S.; Kazanskiy, N.; Butt, M.; Kazmierczak, A.; Piramidowicz, R. Plasmonic sensor based on metal-insulator-metal waveguide square ring cavity filled with functional material for the detection of CO_2 gas. *Opt. Express* **2021**, *29*, 16584–16594. [CrossRef]
200. Luan, E.; Yun, H.; Ma, M.; Ratner, D.; Cheung, K.; Chrostowski, L. Label-free biosensing with a multi-box sub-wavelength phase-shifted Bragg grating waveguide. *Biomed. Opt. Express* **2019**, *10*, 4825–4838. [CrossRef]

201. Liang, Y.; Liu, Q.; Wu, Z.; Morthier, G.; Zhao, M. Cascaded-Microrings Biosensors Fabricated on a Polymer Platform. *Sensors* **2019**, *19*, 181. [CrossRef]
202. Azuelos, P.; Girault, P.; Lorrain, N.; Poffo, L.; Guendouz, M.; Thual, M.; Lemaitre, J.; Pirasteh, P.; Hardy, I.; Charrier, J. High sensitivity optical biosensor based on polymer materials and using the Vernier effect. *Opt. Express* **2017**, *25*, 30799–30806. [CrossRef]
203. Han, X.; Han, X.; Shao, Y.; Wu, Z.; Liang, Y.; Teng, J.; Bo, S.; Morthier, G.; Zhao, M. Polymer integrated waveguide optical biosensor by using spectral splitting effect. *Photonic Sens.* **2017**, *7*, 131–139. [CrossRef]
204. Melnik, E.; Strasser, F.; Muellner, P.; Heer, R.; Mutinati, G.; Koppitsch, G.; Lieberzeit, P.; Laemmerhofer, M.; Hainberger, R. Surface modification of integrated optical MZI sensor arrays using inkjet printing technology. *Procedia Eng.* **2016**, *168*, 337–340. [CrossRef]
205. Leal-Junior, A.; Macedo, L.; Frizera, A.; Pontes, M.J. Polymer Optical Fiber Multimaterial: Flexible and Customizable Approach in Sensors Development. *IEEE Photonics Technol. Lett.* **2022**, *34*, 611–614. [CrossRef]
206. Bahin, L.; Tourlonias, M.; Bueno, M.-A.; Sharma, K.; Rossi, R.M. Smart textiles with polymer optical fibre implementation for in-situ measurements of compression and bending. *Sens. Actuators A Phys.* **2023**, *350*, 114117. [CrossRef]
207. Woyessa, G.; Pedersen, J.K.; Nielsen, K.; Bang, O. Enhanced pressure and thermal sensitivity of polymer optical fiber Bragg grating sensors. *Opt. Laser Technol.* **2020**, *130*, 106357. [CrossRef]
208. Wei, H.; Chen, M.; Krishnaswamy, S. Three-dimensional-printed Fabry–Perot interferometer on an optical fiber tip for a gas pressure sensor. *Appl. Opt.* **2020**, *59*, 2173–2178. [CrossRef]
209. Liu, Y.; Liu, X.; Zhang, T.; Zhang, W. Integrated FPI-FBG Composite All-Fiber Sensor for Simultaneous Measurement of Liquid Refractive Index and Temperature. *Opt. Lasers Eng.* **2018**, *111*, 167–171. [CrossRef]
210. Chen, M.; He, T.; Zhao, Y.; Yang, G. Ultra-Short Phase-Shifted Fiber Bragg Grating in a Microprobe for Refractive Index Sensor with Temperature Compensation. *Opt. Laser Technol.* **2023**, *157*, 108672. [CrossRef]
211. Korganbayev, S.; Sypabekova, M.; Amantayeva, A.; González-Vila, Á.; Caucheteur, C.; Saccomandi, P.; Tosi, D. Optimization of Cladding Diameter for Refractive Index Sensing in Tilted Fiber Bragg Gratings. *Sensors* **2022**, *22*, 2259. [CrossRef] [PubMed]
212. Voronkov, G.; Zakoyan, A.; Ivanov, V.; Iraev, D.; Stepanov, I.; Yuldashev, R.; Grakhova, E.; Lyubopytov, V.; Morozov, O.; Kutluyarov, R. Design and Modeling of a Fully Integrated Microring-Based Photonic Sensing System for Liquid Refractometry. *Sensors* **2022**, *22*, 9553. [CrossRef] [PubMed]
213. Voronkov, G.; Aleksakina, Y.; Ivanov, V.; Zakoyan, A.; Stepanov, I.; Grakhova, E.; Butt, M.; Kutluyarov, R. Enhancing the Performance of the Photonic Integrated Sensing System by Applying Frequency Interrogation. *Nanomaterials* **2023**, *13*, 193. [CrossRef] [PubMed]
214. Han, X.; Ding, L.; Tian, Z.; Song, Y.; Xiong, R.; Zhang, C.; Han, J.; Jiang, S. Potential New Material for Optical Fiber: Preparation and Characterization of Transparent Fiber Based on Natural Cellulosic Fiber and Epoxy. *Int. J. Biol. Macromol.* **2023**, *224*, 1236–1243. [CrossRef]
215. Islam, M.D.; Liu, S.; Boyd, D.A.; Zhong, Y.; Nahid, M.M.; Henry, R.; Taussig, L.; Ko, Y.; Nguyen, V.Q.; Myers, J.D.; et al. Enhanced mid-wavelength infrared refractive index of organically modified chalcogenide (ORMOCHALC) polymer nanocomposites with thermomechanical stability. *Opt. Mater.* **2020**, *108*, 110197. [CrossRef]
216. Afroozeh, A.; Zeinali, B. Improving the Sensitivity of New Passive Optical Fiber Ring Sensor Based on Meta-Dielectric Materials. *Opt. Fiber Technol.* **2022**, *68*, 102797. [CrossRef]

Disclaimer/Publisher's Note: The statements, opinions and data contained in all publications are solely those of the individual author(s) and contributor(s) and not of MDPI and/or the editor(s). MDPI and/or the editor(s) disclaim responsibility for any injury to people or property resulting from any ideas, methods, instructions or products referred to in the content.